DOKUZ EYLÜL UNIVERSITY
GRADUATE SCHOOL OF NATURAL AND APPLIED SCIENCES

SYSTEM-LEVEL MODELING AND SIMULATION OF DIRECT METHANOL FUEL CELLS

by
Alper Can İNCE

June, 2019
İZMİR

SYSTEM-LEVEL MODELING AND SIMULATION OF DIRECT METHANOL FUEL CELLS

A Thesis Submitted to the
Graduate School of Natural and Applied Sciences of Dokuz Eylül University
In Partial Fulfillment of the Requirements for the Master of Science of
Department of Mechanical Engineering

by

Alper Can İNCE

June, 2019
İZMİR

M.Sc THESIS EXAMINATION RESULT FORM

We have read the thesis entitled **"SYSTEM-LEVEL MODELING AND SIMULATION OF DIRECT METHANOL FUEL CELLS"** completed by **ALPER CAN İNCE** under supervision of **ASSOC. PROF. DR. CAN ÖZGÜR ÇOLPAN** and we certify that in our opinion it is fully adequate, in scope and in quality, as a thesis for the degree of Master of Science.

Assoc. Prof. Dr. Can Özgür ÇOLPAN

Supervisor

Prof. Dr. Aytunç EREK

(Jury Member)

Assist. Prof. Dr. Ebru ERÜNAL

(Jury Member)

Prof.Dr. Kadriye ERTEKİN
Director
Graduate School of Natural and Applied Sciences

ACKNOWLEDGMENT

The author wishes to express deep gratitude to co-supervisors Assoc. Prof. Dr. Can Özgür ÇOLPAN and Assoc. Prof. Dr. Mustafa Fazıl SERİNCAN for their invaluable supervision, advice, encouragement, support, and insight throughout the research process.

The author wishes to express her special thanks to his dear friends Yağmur NALBANT, Anıl ERDOĞAN and Mustafa KARAOĞLAN for his valuable contributions in this study.

The author thanks to Institute of Energy and Climate Research IEK-3: Electrochemical Process Engineering, (Jülich Forschungzentrum, Germany) and especially to Andreas GLUSEN and Martin MULLER, for the labaratovuary facilities.

The author gratefully thanks to her parents Azime İNCE and Bekir İNCE, specially his brother Mustafa İNCE and his sister Özlem İNCE for their invaluable support in her entire life.

Alper Can İNCE

SYSTEM-LEVEL MODELING AND SIMULATION OF DIRECT METHANOL FUEL CELLS

ABSTRACT

In this thesis, a thermodynamic model of an active direct methanol fuel cell (DMFC) system, which couples in-house experimental data for the DMFC with the equations of the mass, energy and exergy balances for the system components, is developed. For this purpose, the thermodynamic analysis is developed by following; firstly, a semi-empirical mathematical DMFC system model which is less costly than fully experimental methods and more accurate than fully theoretical methods, is formed. Secondly, the empirical data which are obtained with experiments on DMFC for some operating conditions (e.g. methanol concentration, current density and air flow rate) are integrated to the model equations (mass, energy and exergy balances) through curve fitting method. Thus, this model gives the mass and exergy flow rates at the inlet and exit of the anode and cathode sides as well as power density of DMFC. The basic thermodynamic equations are then applied around control volume enclosing system components of DMFC to find mass flow rates and exergy flows at the inlet and exit of these components. Solving these equations in Engineering Equation Solver (EES), the effect of operating conditions on the condenser outlet temperature, exergy destruction of each component, the required power of system components, electrical and exergetic efficiency of DMFC system is calculated. Moreover, water autonomy for this system is examined through a novel two-phase condenser model developed. The comprehensive results (e.g. relative humidity and mole fraction) as well as condensate mass flux in the condenser are obtained through this model for water autonomy.

Keywords: Direct methanol fuel cell system, semi-empirical, mathematical model, energy, exergy, water autonomy, condenser, two-phase

DOĞRUDAN METANOLLÜ YAKIT PİLLERİNİN SİSTEM-DÜZEYİ MODELLEMESİ VE SİMÜLASYONU

ÖZ

Bu tezde, doğrudan metanollü yakıt pili (DMYP) için kurum içi deneysel verilerini, sistem elemanları için uygulanan kütle, enerji ve ekserji denge denklemleriyle birleştiren aktif DMYP sisteminin termodinamik bir modeli geliştirildi. Bu amaçla, termodinamik analizi takip eden şekilde geliştirilmiştir; ilk olarak, tamamen deneysel yöntemlerden daha az maliyetli ve tamamen teorik yöntemlerden daha doğru olan yarı-deneysel bir matematiksel DMYP sistemi modeli oluşturulmuştur. Bu amaçla, bazı çalışma koşulları (örneğin metanol konsantrasyonu, akım yoğunluğu ve hava akış hızı) için DMYP üzerinde yapılan deneylerle elde edilen veriler, eğri uydurma yöntemi ile model denklemlerine (kütle, enerji ve ekserji dengeleri) entegre edilmiştir. Böylelikle, bu model, çalışma koşulları altında anot ve katot taraflarının giriş ve çıkışındaki kütle akış hızlarını, ekserji akış hızlarının yanı sıra DMYP'nin güç yoğunluğunu bulmak için kullanılır. Daha sonra, sistem elemanlarının giriş ve çıkışındaki kütle ve ekserji akış hızlarını bulmak için temel termodinamik denklemler bu sistem elemanlarını çevreleyen kontol hacimlerine uygulanır. Bu denklemler Engineering Equation solver (EES)'da çözülerek, çalışma koşullarının kondenser çıkış sıcaklığına, her bir sistem elemanı için ekserji yıkımlarına, sistem elemanlarının güç çıktısına ve sistemin elektriksel ve ekserjetik verimliliğine etkisi hesaplanmıştır. Ayrıca, bir DMYP sisteminde kurulu hazır bir kondenser için iki fazlı yenilikçi bir model geliştirilerek bu sistemin su özerkliği incelenmiştir. Su özerkliği için bu modelden kapsamlı sonuçlar (örneğin bağıl nem ve buhar basıncı) ve kondenserdeki yoğuşmuş kütle akısı elde edilir.

Anahtar kelimeler: Doğrudan metanollü yakıt pili sistemi, yarı deneysel, modelleme, matematiksel model, enerji, ekserji, su özerkliği, kondenser, iki faz

CONTENTS

Page

LIST OF FIGURES

Page

LIST OF TABLES

Page

CHAPTER ONE
INTRODUCTION

1.1 Introduction

The energy demand of the world has been increased last decades due to the increase of human population and industrialization. Fossil fuels which consist of oil (33.7 %), natural gas (23.6%) and coal (29.7%) are used by 87 % to meet this energy demand. However, these fuels are considered as non-renewable energy, major cause of global warming and descending its reservoir. For these reasons, the development of the alternative energy conversion technologies has increased (Corti & Gonzalez, 2014).

Due to the increasing these concerns on environmental problems (e.g. climate change and air pollution) and diminishing petroleum reserves, fuel cells (FCs), which converts chemical energy to electricity and generally offer better environmental impact, have become popular for applications ranging from portable to hybrid vehicular (e.g. Polymer electrolyte membrane (PEM) fuel cells) to power plants (e.g. Solid oxide fuel cells (SOFCs)) in the recent years as energy conversion device. Fuel cells are promising technologies because of having high electrical efficiency, no moving part and low environmental impact when compared to traditional power technologies such as internal combustion engines and gas turbines which work dependence on fossil fuels. In addition, unlike a battery which another important energy conversion device, there is no need to recharge the fuel cells when the fuel is supplied continuously.

Fuel cells can be classified following main types according to the materials of construction, type of ion, and the type of fuel used: PEM fuel cells, direct methanol fuel cells (DMFCs), molten carbonate fuel cells (MCFCs), SOFCs, alkaline fuel cells (AFCs) and phosphoric acid fuel cells (PAFCs) (Y. Wang, Chen, Mishler, Cho, & Adroher, 2011). They vary in terms of power output, operating temperatures and types of applications. DMFCs are more convenient for portable and hybrid vehicular applications as they can be used at low operating temperatures, and they have easy fuel

storage and no fuel process system unlike other fuel cell types. However, heat and water management are crucial challenges as well as undesired methanol permeation. To mitigate these negative effects, the DMFC system models have been developed. The DMFC system that is considered in this study consists of a condenser, three pumps, a mixing chamber, a blower, and a methanol tank.

In this thesis, a semi-empirical thermodynamic model of an active direct methanol fuel cell (DMFC) system, which couples in-house experimental data for the DMFC with the mass, energy and exergy balances for the system components (condenser, mixing vessel, blower and pumps), is formed to enhance system performance. The modeling equations are solved using the Engineering Equation Solver (EES) program. Furthermore, a novel approach which is a more comprehensive method than the fully theoretical method and more time-saving than the fully two-phase model is proposed. Using this model, results for relative humidity, vapor pressure and mole fraction in the condenser are obtained. In addition, the required condensate mass flux of DMFC system for water autonomy calculated with some assumptions and generalizations is compared with the condensate mass flux of available condenser calculated with an alternative two-phase model.

1.2 Motivation

This thesis focuses on the modeling and simulation of DMFC at system levels. The main novelty is to propose a new semi-empirical mathematical approach, which is less costly than fully experimental methods and more accurate than fully theoretical methods, to design and analyze DMFC systems. In the literature, although there are a few studies on the semi-empirical modeling of DMFCs on cell-level, according to the authors' knowledge, there are no studies on system-level (including BOP components) using this kind of modeling approach. For this reason, a semi-empirical mathematical model of a DMFC system is developed in this study, coupling detailed mass and energy and exergy balances with in-house experimental data including the polarization, methanol crossover, and water crossover curves of the DMFC. In addition, the condenser is modeled with an approach with critical assumptions in the

DMFC system simulations according to literature survey. This approach leads to some limitations in the analysis of the DMFC system. Therefore, in this study, a novel approach which is a more comprehensive method than the method includes critical assumptions, generalizations and simplifications, and more time-saving than the fully two-phase model is proposed to investigate temperature, vapor pressure and relative humidity distribution and condensate mass flux in condenser for water autonomy. Hence, the condensate mass flux obtained from available condenser is compared with the condensate mass flux obtained from the system requirements.

1.3 Objective

The main aim of this thesis is to develop a semi-empirical mathematical model, data obtained from the DMFC experiments such as methanol crossover current density, water crossover rate and cell voltage, are implemented in the thermodynamic model of the DMFC system. This model gives the mass flux at the inlet and outlet of the anode and cathode sides, and the heat loss and power density of the DMFC. Mass, energy and exergy balances are then applied around the control volumes enclosing the BOP components to find the thermodynamic properties of each state and heat and work interactions between the system and its surroundings. Another important aim is to provide water autonomy (water management) for DMFC system via condenser. For this purpose, a novel two-phase thermal model for an available condenser in DMFC system is developed.

1.4 Thesis Outline

The Chapter 2 is represented to the general information about the fuel cell based on system and cell level, especially Direct Methanol Fuel Cell Systems. Chapter 2 gives the information about fuel cell main components (electrolyte, electrodes), promising fuel cell types (DMFC, PEM and SOFC), fuel cell system configurations and components (pumps, humidification, blower, condenser, mixing vessel, compressor), and includes the literature review. In this review, studies (experimentally and numerically) on DMFC system, stack and cell level basis, and the semi-empirical

models of cell and stack level of DMFC are discussed. The third chapter denotes the performance test which includes polarization, methanol crossover current density and water crossover curves followed for single cell and short stack of DMFC in more detail. Furthermore, the results of experiment are given in this chapter. The fourth chapter explains how to couple system-level mathematical model with thermodynamic model of the DMFC. In addition, thermodynamic model for the DMFC system (including BOP components) is then presented, and energy and exergy analyses are given as well as two-phase method of condenser for water autonomy. In the fifth chapter, the results of the semi-empirical thermodynamic DMFC system model and a two-phase mathematical model for condenser are given and discussed in detail. The sixth chapter gives conclusions related to the studies in this thesis.

CHAPTER TWO
BACKGROUND AND LITERATURE REVIEW

2.1 Fuel Cells

Fuel cells are considered as energy conversion devices which convert chemical energy into electricity through high-efficiency. The fuel cell is composed of two-electrodes (anode and cathode) and electrolyte, which are called Membrane Electrode Assembly (MEA). The electrochemical oxidation and reduction reactions are formed anode and cathode electrodes, respectively. The fuel cells simply work as following: As a result of oxidation reaction at the anode electrodes, electrons generated are transferred to cathode catalyst by following external circuit while ions produced migrate to cathode side through the electrolyte. Ions and electrons recombine and react with oxygen which is called oxygen reduction reaction (ORR) at the cathode side, and fuel cell electrical power, heat and chemical products are generated.

The fuel cell types have been developed considering lack of operational issues in practice (e.g. slow kinetic reaction rate, low power, material and fuel available). These types are classified as Proton Exchange Membrane (PEM), Direct Methanol Fuel Cell (DMFC), Alkaline Fuel Cell (AFC), Molten Carbonate Fuel Cell (MCFC) and Solid Oxide Fuel Cell (SOFC) according to their characteristics (the materials of electrolyte, mobile ion, operating temperature, fuel type used) which are given in Table 2.1 (Mench, 2008). Also, their system application fields are shown in Figure 2.1. Especially, SOFC, PEM and DMFCs are widely commercialized last decades (Barbir, 2012).

Table 2.1 Types of important fuel cells and their basic data (Adapted from Mench, 2008)

	DMFC	**AFC**	**PEMFC**	**SOFC**	**MCFC**
Operating Temperature, °C	60-80	60-220	60-200	600-1000	~650
Typical Electrolyte Material	Polymer Membrane	Potassium hydroxide in water	Polymer Membrane	Ceramic	Molten Carbonate
Ion types	H^+	OH^-	H^+	O^{2-}	CO_3^{2-}
Typical Fuel	CH_3OH	H_2	H_2	H_2, CH_4, CO	H_2, CH_4
Poison	Metal ions	CO_2	CO, Sulfur	Sulfur	Sulfur

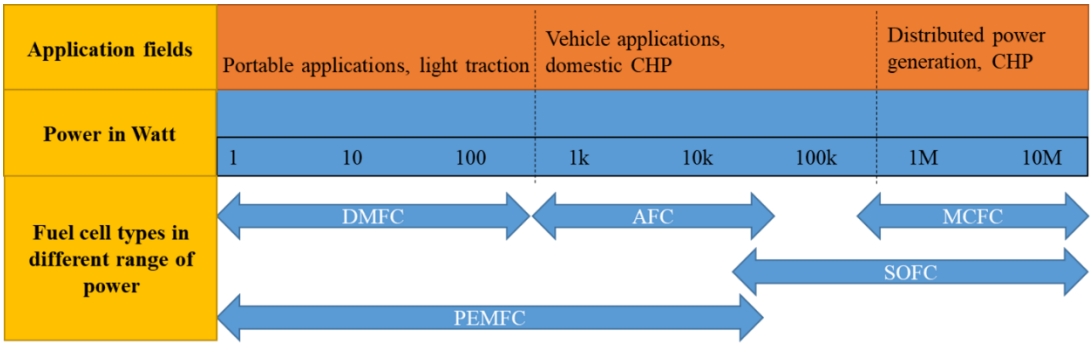

Figure 2.1 Fuel cell types in different range of power and typical applications (Adapted from Larminie and Dicks, 2003)

2.2 Direct Methanol Fuel Cells (DMFCs)

In the DMFC, in addition to the generated power, carbon dioxide (CO_2) and water are produced at the anode side, whereas part of the O_2 and water is consumed at the cathode side as a result of the reactions shown in Eqs. (2.1) and (2.2). A portion of methanol permeates (CH_3OH_{perm}) to the cathode, mainly owing to the diffusion of methanol through the membrane; and CO_2 and water are formed at the cathode as shown in Eq. (2.3) (Dohle & Wippermann, 2004). Similarly, a portion of water permeates to the cathode due to electro-osmosis, hydraulic permeation, and diffusion (Lu, Wang, Yen, & Zhang, 2004). Excess methanol and water leaving the anode side enter the mixing chamber, together with CO_2 generated at the anode. CO_2 is then released into the atmosphere from the top of this chamber. On the other hand, two-phase water and dry gas composed of CO_2, O_2 and N_2 leave the cathode side of the DMFC.

As the polymer electrolyte membrane, like proton exchange membrane fuel cells (PEMFCs), are used in the DMFCs, the DMFC is considered as a type of the PEMFCs. However, DMFCs, unlike PEMFC, vary in terms of operating temperature, fuel used, and catalyst type. In general, as the DMFCs use a liquid methanol solution, which carries some important advantages, such as high energy density, low cost and easy storage and handling of fuel when compared to PEMFCs. In addition, as it operates at comparatively low temperatures (70-80 °C), it has a quicker start-up and fewer issues with manufacturing and insulation when compared to high-temperature fuel cells, such as solid oxide fuel cells (SOFCs).

$$\text{Anode: } CH_3OH + H_2O \rightarrow CO_2 + 6H^+ + 6e^- \quad (2.1)$$

$$\text{Cathode: } \frac{3}{2}O_2 + 6H^+ + 6e^- \rightarrow 3H_2O \quad (2.2)$$

$$\text{Overall: } CH_3OH + \frac{3}{2}O_2 \rightarrow CO_2 + 2H_2O \quad (2.3)$$

However, fuel and voltage losses due to methanol permeation (Cruickshank & Scott, 1998), the need for high catalyst loading, which increases the materials cost significantly at both electrodes (Sgroi et al., 2016), durability (Müller, Kimiaie, Glüsen, & Stolten, 2014), slow reaction kinetics at both electrodes (Kulikovsky, 2003), water management (Lu, Liu, & Wang, 2004), and thermal management (especially for large stacks) (Faghri & Guo, 2005), are the main challenges facing the widespread use of DMFCs in commercial applications. To diminish these challenges, especially, water and thermal management, the DMFC system applications which can be classified passive and active systems discussed in Section 2.4 in more detail, have been developed by many researcher recent years. Another challenges mostly related with the improvement of MEA which is examined for each component at following Sections (2.3, 2.3.1, 2.3.2, 2.3.3).

2.3 Direct Methanol Fuel Cell and its Components

The MEA which is shown in Figure 2.3, is simply composed of a membrane, two catalyst layers, two diffusion layers, two gaskets, two gas diffusion layers, two separator plates and two current collectors. The brief information about these components are given from Section 2.3.1 to Section 2.3.2.

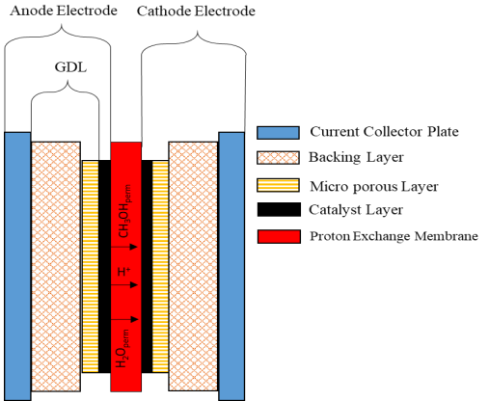

Figure 2.3 The MEA structure

2.3.1 Membrane

In DMFCs, a membrane based on solid polymer, is a considered as barrier between two-electrodes; it allows H^+ ions to pass through but inhibits electrons. The criteria of a DMFC membrane are high proton conductivity, electrical isolation, good chemical and mechanical stability and minimizing methanol and water crossover. In general, Nafion® is the most widely material used in DMFCs due to its good chemical resistance and high conductivity. However, as it has permeability for fuel, the membrane based graphene is the novel materials to replace Nafion® membrane (Shaari & Kamarudin, 2017). In this study, Nafion® is chosen as membrane due to its easy availability.

2.3.2 Anode and Cathode Electrodes

Electrodes are mainly comprised of catalyst layers (CLs), gas diffusion layers (GDLs). While oxidation reaction of the reactant (methanol) occurs at the anode catalyst layer (ACL), the layer where the oxygen reduction reaction (ORR) occurs is cathode catalyst layer (CCL). As the reactions take place in the CLs, the CLs play key role to improve cell performance. Therefore, the expensive noble metals are used in the CLs such as carbon supported or unsupported Pt and Pt-Ru. As well, the preparation of CLs is another important factor on cell performance. Painting, brushing, air spraying and doctor blading are coating methods to build CLs structure. Similarly, the Electrohydrodynamic jet deposition is novel and effective coating methods (L.

Wang et al., 2018). The GDLs include backing layer which is made of carbon paper and porous layer based on carbon black and Nafion® ionomer. The GDLs are considered as a bridge between the catalyst layer and the current collector in terms of the mass and electrical connection (Zhang et al., 2007). In addition, GDLs provide the mechanical support for MEA (Colpan, Ouellette, Glüsen, Müller, & Stolten, 2017).

2.4 DMFC Systems

A DMFC can be designed as a passive or an active system to provide better water and thermal management, and provide lower methanol crossover. In the Section 2.4.1 and 2.4.2, the working principle, advantages and disadvantages, application fields and main components of passive and active systems are given, respectively.

2.4.1 Passive Systems

The working concept of the passive DMFC (which is shown in Figure 2.4) is that the DMFC can be operated unassisted without auxiliary equipment such as pumps, blower/fan/compressor and heat exchangers. Thus, the passive DMFC systems enable to simple design and they have low volume. However, the passive DMFC systems have much lower power output density (per active area 20 mW) due to the problem of its inability to control unreacted water. In addition, high heat loss from the cell to environment leads to reduce power output density (Faghri & Guo, 2008; Chen & Zhao, 2005). In passive systems, a methanol-water solution is delivered to cells with less control over methanol through diffusion owing to a methanol concentration gradient and without the use of pumps. In addition, air flows into the cell by natural convection (Vasanth & Kolar, 2018). These systems, which have been developed by some Japanese and Korean companies, can be used for low-power applications such as personal digital assistant (PDA) devices and mobile phones.

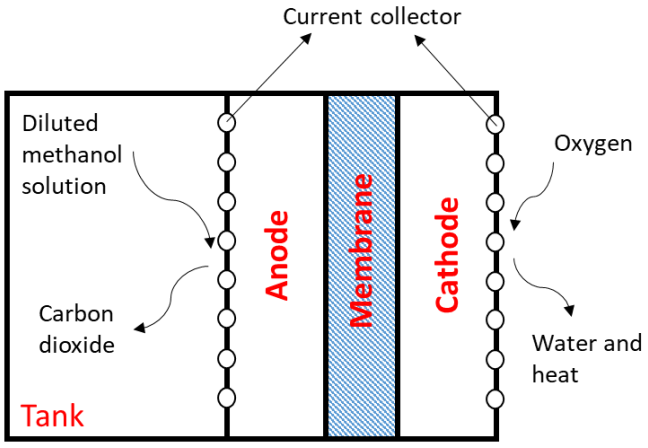

Figure 2.4 A passive DMFC system (Adapted from Chen & Zhao, 2005)

2.4.2 Active Systems

In an active system, a fuel delivery system provides flexibility in system control as the mass flow rate of methanol and air, and the concentration of methanol can be controlled. Hence, the use of an active system enhances fluid mass transport and electrochemical activity, thus and so a higher performance of power output can be achieve (Q. Xu et al., 2018). An active DMFC system generally includes a condenser, an anode mixing vessel, a circulating pump, a condensate pump, a methanol pump, an air blower, and a methanol tank as shown in Figure 2.5. In this system, air reaches the cathode side after passing through an air blower (according to DMFC system requirements, compressor can be used) and an air filter, respectively. At the cathode side, water is generated by the oxygen reduction reaction and the reaction of crossed over methanol with oxygen. Some amount of water also exists at the cathode side because of the water crossover from the anode to the cathode. In addition, CO_2 is produced as a result of methanol reaction with oxygen. The fluid mixture consisting of H_2O, CO_2, N_2, and O_2 leaving the stack is cooled down and water is separated to liquid and gas phases after passing through a condenser which is important component for water autonomy which is discussed Section in 2.5.3, in the system. Then, liquid water is recycled to the anode mixing vessel and methanol reaches the anode mixing vessel from the methanol tank. This diluted methanol solution is pumped to the anode side. Unreacted methanol, CO_2 and water formed in the stack return to the anode

mixing vessel; and CO_2, water vapour, and methanol vapour are released to the atmosphere from the top of the vessel.

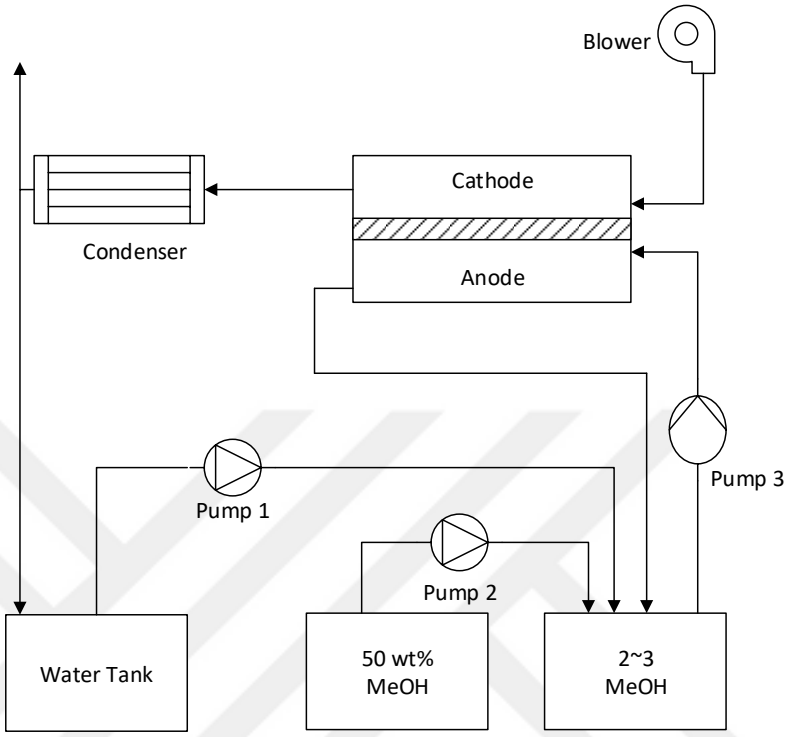

Figure 2.5 An active DMFC system (Adapted from Takaguchi & Ohashi, 2015)

2.5 Literature Survey

2.5.1 DMFC in Cell and Stack Level

In the literature, there are many studies on the development and performance improvement of single DMFCs or DMFC stacks, which include examining the effect of operating parameters (Colpan et al., 2017; Seo & Lee, 2008), the effect of methanol permeation (Choi, Kim, & Woo, 2001), the materials used in membrane electrode assemblies (MEAs) (Ercelik, Ozden, Devrim, & Colpan, 2017), and the flow field and manifold design in cell and stack levels (Ozden et al., 2017; Li & Faghri, 2013).

There is a strong literature based on numerical (theoretical) modeling which includes mass and energy transport phenomena of DMFCs and its coupling with electrochemical model in cell and stack level. Gwak, Kim, Lee, & Ju (2018) performed comparatively

study on a high-temperature DMFC based on PBI membrane and PFSA membrane to investigate the methanol crossover and cell voltage using one-dimensional model. Their simulation showed that the minimum methanol crossover rate is achieved at methanol concentrations higher than 12 M and they validated the results of their numerical model with experimental data that were taken over a wide range of methanol concentrations and current densities. Ramesh & Krishnamurthy (2018) also used a one-dimensional model to find the change of temperature distribution and heat generation for catalyst layer, backing layer of anode and cathode and membrane layer with time in a DMFC. In their model results, a higher temperature profile which is resulted of higher heat generation, is found at the cathode with increasing anode flow rate and methanol concentration and current density. In addition, they found that the required time to reach steady-state is forty-five minutes. Ismail, Kamarudin, Daud, Masdar, & Hasran, (2018) developed a two-dimensional non-isothermal and transient mass transfer model for each layer of a DMFC to determine the cell performance at various operating temperature and methanol concentration. The optimization of power output is then studied. Finally, the results show that the optimized power output is found as 48 $mW \cdot cm^{-2}$ which corresponds to voltage and current density values of 0.26 V and 190 $mA \cdot cm^{-2}$, respectively. Sun, Zhang, Guo, Jiao, & Huang, (2018) developed a three-dimensional model to investigate gas and liquid two-phase flow in channels and porous electrodes of a DMFC as a function of operating temperature, methanol concentration, and current density. They showed that the CO_2 which is obtained as a result of methanol oxidation reaction accumulates at the between of GDL and anode channel.

The semi-empirical model is an effective approach to provide better and easier understanding of relationships between the cell performance and cell operating conditions (Yang, Kianimanesh, Freiheit, Park, & Xue, 2011). The semi-empirical model approaches which is less costly than fully experimental methods and more accurate than fully theoretical (numerical) methods were applied for determining the performance of DMFCs in some studies. For example, Argyropoulos, Scott, Shukla, & Jackson (2003) developed a model to predict the cell voltage of a DMFC using the semi-empirical method, and they also validated their study with experimental data. They

reported that the model can be used for various range of MEA. Dohle & Wippermann, (2004) conducted semi-empirical modeling of a DMFC to find its performance and methanol permeation under different operating conditions. For this purpose, they first determined cell voltage, anode potential and methanol permeation experimentally. These data obtained experimentally are then used as a set parameter for DMFC model. Chiu, Yu, & Chung (2011) developed a semi-empirical model to evaluate the efficiency and power density of the DMFC, which are functions of cell temperature, methanol concentration, and current density. Yang et al. (2011) investigated the relationships between operating conditions (temperature, methanol concentration, and anode and cathode flow rates) and performance of a DMFC through a semi-empirical model.

2.5.2 DMFC in System Level

The studies on the modeling and development of DMFCs at the active system level are insufficient. However, there are many studies on the passive system in the literature. The studies where the researchers conducted on construction and analysis (e.g. mass, energy and exergy) of passive DMFC is given following. Jewett, Faghri, & Xiao (2009) optimized a passive DMFC to determine air management system, methanol concentration feed and membrane thickness using numerical simulation developed in some of authors' previous study (Rice & Faghri, 2006; Xiao & Faghri, 2008). The important finding in their study was that when the Oil Sorbents air filter is used for air management system of passive DMFC, the efficiency of fuel utilization is enhanced by 27.35 %, and the maximum power density is decreased by 10.18 %. Guo & Cao (2004) developed a transient model based on two-phase to investigate the effect of the MEA design on the performance of passive DMFC. Consequently, it was obtained that the 117 Nafion® membrane is better type of membrane for passive DMFC in terms of efficiency of fuel and energy, and energy density when compared to 112 and 115 membranes. Bahrami & Faghri (2010) first developed analytical model passive DMFC to find water, methanol crossover and cell voltage. The exergy analysis on passive DMFC was then studied to determine entropy generations inside cell. Finally, they reported that the mostly exergy destruction is occurred due to methanol crossover. In addition, lower methanol concentration provides a better exergy efficiency (second-law efficiency).

In active systems, for example, the steady-state simulation of the DMFC systems was released by Andrian & Meusinger, 2000 who investigated DMFC system performance under operating conditions (e.g. cell temperature, cell pressure, air to fuel ratio, and methanol crossover). It was obtained that a better system electrical efficiency with a reducing the air to fuel ratio. Besides, it was found that when the methanol crossover increases, the DMFC system electrical efficiency reduces significantly. Dohle, Mergel, & Stolten (2002) performed study on thermal management in a DMFC system, which includes a DMFC, a compressor-expander unit, a catalytic exhaust treatment, pumps and a heat exchanger. Solving the energy and mass equations applied around the control volumes enclosing auxiliary equipment under various working conditions, they demonstrated that overall system efficiencies (the product of the efficiency of fuel cell and the auxiliary system components) as high as 35% could be achieved. Mergel, Janßen, Müller, Wilhelm, & Stolten (2012) investigated the durability of a DMFC system at the IEK-3, Forschungszentrum Jülich. Takaguchi & Ohashi (2015) presented the development of a 1 kW commercial DMFC system which is shown Figure 2.5. This system consists of a DMFC stack with a Z-flow configuration, a water tank that collects recycled water, a 50 wt % methanol tank, a 2-3 wt % methanol tank that is used as a mixing vessel, three pumps, a fan, and a heat exchanger at the cathode outlet. In the system, hot water at 50 °C can be generated for domestic applications, as well as generating electricity. They found that the utilization of fuel for DMFC reaches 80% at the power ratio which is described as the ratio between the DMFC's output power and rated power of 1. Lee, Lee, Han, Gwak, & Ju (2017) conducted simulation of the DMFC active system under various operating conditions to show system behavior. To do this, a one-dimensional analytical model of a DMFC that was validated experimentally through the study of Ko et al. (2011) was developed to find mass transport phenomena inside cell (e.g. water diffusion, water permeation, water drag, and methanol crossover). These data are then implemented in an active system model, which consists of system equipment (i.e., pumps and blowers) and heat exchangers. Using this model, the heat management in the system was analyzed, and the power consumptions of system components were found. According to their study, the temperature of anode inlet is found as between 70 and 80 °C. The range of this temperature provides an enhancement

in the power density of DMFC. In addition, the increasing of anode inlet temperature results in decreasing power consumptions by the system equipment.

Exergy analysis is a tool that can be used to find the locations and magnitudes of exergy destructions (a measure of irreversibilities) within thermodynamic systems. There are few studies on the exergy analysis of PEMFCs (e.g. Leo, Durango, & Navarro, 2010), SOFCs (e.g. Colpan, 2012), and DMFCs (e.g. Hotz, Lee, Grigoropoulos, Senn, & Poulikakos, 2006). Li, He, Yin, Miao, & Li (2008) expressed the effect of various working conditions (e.g. methanol cross-over rate, cathode pressure, methanol concentration and temperature) on total exergetic efficiency of DMFC system. In their results, the better total exergetic efficiency occurs at higher current density, lower methanol concentration and higher cathode pressure. However, some of operating conditions are limited due to fabrication, sealing, life time and maintenance of stacks. The other study on exergy analysis for DMFC system was examined by Wu & Lin, 2010. They developed fuzzy-based multi-objective optimization algorithm to find optimum operating parameters for the better exergetic DMFC system performance and fuel efficiency. To do this, they developed dynamic and non-isothermal model for the DMFC system based on experimental model. Consequently, they investigated exergetic efficiency, electrical efficiency and fuel efficiency according methanol concentration, load demand and anode inlet temperature. Osat, Nejad, Sedighi, Farhadi, & Asghari (2014) presented study of exergy analysis of DMFC at various current density, temperatures, pressures and cell voltages. They found that the exergetic efficiency increase with an increasing voltage. In addition, the optimum current density was found between of 0.40 $A \cdot cm^{-2}$ and 0.55 $A \cdot cm^{-2}$ to obtain peak exergetic efficiency.

2.5.3 Water autonomy in DMFC system

Water management plays critical role in DMFCs to utilize energy level of methanol and to prevent water floods at cathode. So far, many studies on water management reported in the literature (Oliveira, Rangel, & Pinto, 2009; Xu & Zhao, 2007; Liu & Wang, 2008). These studies mostly related to DMFC cell design. However, the effect of system design on water management is demonstrated in only a few studies following as:

Zenith, Weinzierl, & Krewer (2010) developed a model that includes mass balance equations for the DMFC system components. The DMFC system's water autonomy was investigated for various operating conditions. The results indicated that the autonomy mainly depends on three variables: the environmental humidity, the temperature of the condenser, and the air flow rate. Jiang & Chu (2006) examined the recycled water percentage under cell operating conditions through a system-level model. For this purpose, water crossover data obtained from a DMFC stack model was used. Their results indicated that 98% of the water from the cathode outlet must be recycled at an average cell voltage of 0.33 V and a cell temperature 62 °C. Janssen et al., (2010) investigated water management in actual DMFC system. They reported that the heat rejection from the DMFC stack is transferred to the stack outlet gas through evaporation of water. They first calculated the mass flow rate of water evaporation. The condenser size was then determined to provide water autonomy. Finally, they calculated condenser outlet temperature for water autonomy. Schultze & Horn (2012) developed a dynamic model of the PEMFC system to determine a better efficient system operation. A stationary model (approximation) based on the effectiveness-NTU method of the counter-flow condenser was developed. The model assumes that condenser inlet and outlet are fully saturated. They found the outlet temperature of hot and cold gas in the condenser to calculate vapor and liquid mass flow rate leaving the condenser. Nölke (2007) presented a study on DMFC system analysis for 5 kW vehicular (scooter) application. In the study, the sizing optimization first conducted for the condenser. Then, the analytical model of this condenser which gives pressure drop through the cooling channel and the condenser outlet temperature of hot gas for variable types of fin and cell temperatures was performed. As a result, the size of the condenser was determined as 170x170x150 m^3, and the condenser outlet temperature was found 40°C when the cell temperature is 70 °C. In addition, the highest pressure drops, and the lowest heat transfer coefficient was calculated at the rectangular fin type for air channel.

In the literature, although there are a few studies on the semi-empirical modeling of DMFCs on cell and stack-level, according to the authors' knowledge, there are no studies on system-level (including water autonomy management) using this kind of modeling approach (Ince et al., 2019). For this reason, a semi-empirical mathematical

model of a DMFC system is developed in this study, coupling detailed mass and energy balances with in-house experimental data including the polarization, methanol crossover, and water crossover curves of the DMFC. In addition, in the literature survey discussed in Section 2.5.3, the condenser is modeled with some assumptions and generalizations to investigate water autonomy. It causes to some limitations in the analysis of the DMFC system. In this study, a novel two-phase mathematical model is developed to investigate condenser in detail for water autonomy.

CHAPTER THREE
EXPERIMENTAL STUDY

3.1 Introduction

The procedure followed in the performance tests of single cell and short stack of DMFC is presented in this chapter. As empirical data were used as the input parameters for the system-level model discussed in Chapter 4, experiments to obtain the polarization curve as well as the methanol and water crossover curves according to air flow rate, current density and methanol concentration were carried out at single cell experimental test setups which were custom-made at the Forschungszentrum Jülich. Similarly, experiments to obtain polarization curves for the short stack according to air flow rate, methanol permeation and current density were conducted at short stack experimental test setups at the same institution. Consequently, the comparison of the performance results between single cell and short stack were performed to understand abilities of each of the two approach in terms of DMFC characterization. For this purpose, the single cell test rig conditions are rearranged according to the short stack results for the comparison.

It should be noted that the system simulation was done for single cells (unarranged according to short stack) rather a DMFC stack due to the limitations in the experimental facilities to obtain the necessary data, which include the methanol and water crossover rates. When a single cell is considered rather than a stack, the main assumption in the modelling is that all cells have the same behaviour. However, cells located close to the end plates would behave slightly different than the ones located in the middle. In addition, the maintaining the cell temperature constant within the cells would be challenging in the DMFC stack (Mench, 2008).

3.2 Experiment of DMFC in cell level

To obtain empirical data, the experimental single-cell test setup, which is illustrated in Figure 3.1, was used. This was custom-made at the Forschungszentrum Jülich. This

test setup can control the cell's operating temperature and the anode and air flow rates via a peristaltic pump and mass flow controller. Methanol concentrations can be adjusted up to 3 M by mixing appropriate quantities of pure water and methanol from 0.75 M or 3 M methanol tanks using a three-channel pump, whereby the channels can be independently operated. The system has a DC electronic load to control and consume the required current, with cell voltage measured by a digital voltmeter. In addition, at the cathode outlet, the system includes a heater, an evaporator (to evaporate all the liquid water at the cathode outlet), a humidity sensor (to detect water vapor), a condenser (to collect liquid water) and a CO_2 sensor (to measure the CO_2 concentration).

A membrane electrode assembly (MEA) of DMFC from Johnson Matthey Fuel Cells (specification name: MEA 0630) with 4.2 cm x 4.2 cm of active area was sealed on both the anode and cathode sides by the use of a 0.2 mm-flat gasket made of polytetrafluoroethylene (PTFE). The end plate was made of stainless steel with the dimensions of 12 mm x 90 mm x 90 mm. The anode and cathode flow fields had a checkerboard structure with 1 mm as the width and depth of the channels, as well as the width of the lands. The flow fields were machined from graphite-filled phenolic resin composites (BBP4). The break-in procedure was first conducted to obtain a stable cell performance. For this purpose, methanol was fed to the anode side after it is heated up to 70 °C for 2 h without drawing the current to stabilize and obtain the operating cell temperature inside the heating cell. If the cell voltage at any current density is lower than 0.1 V, the step is automatically skipped by the test station software to prevent corrosion of the anode catalyst. The measurements took 1 h at each time step to ensure reliable values for the water crossover rate. Finally, at the end of the measurement, the cell was cooled down to 30 °C over 2 h without any current to prevent damage to the catalysts.

After the break-in procedure, the performance tests were carried out at different current densities of between 0.05 and 0.25 $A \cdot cm^{-2}$, with an increment of 0.05 $A \cdot cm^{-2}$. The fuel cell temperature and operating pressure were taken as 70 °C and 1 atm, respectively. A diluted methanol solution was fed to the anode side with a flow rate of

0.23 mL·cm^{-2}·min^{-1} at different concentrations (0.5 M, 0.75 M, 1 M, and 1.25M). Dry air at ambient pressure was then fed to the cathode side with different flow rates (20 mL·cm^{-2}·min^{-1} and 30 mL·cm^{-2}·min^{-1}). During the tests, the cathode outflow gases were heated up to 130 °C by an evaporator to ensure that all the water at the cathode outlet is in the vapour phase. Here, permeated water was detected by a humidity sensor. The cathode outflow gas was then sent to the condenser in order to separate the water and CO_2. The CO_2 concentration was measured by a CO_2 sensor attached to the top of the condenser. As the CO_2 is generated due to the fact that permeated methanol reacts with oxygen, the measured CO_2 gives the molar flow rate methanol permeation. To calculate methanol permeation from the CO_2-concentration in the cathode exhaust, it must be assumed that all permeated methanol is oxidized to CO_2 at the cathode (Colpan et al., 2017; Ren, Springer, & Gottesfeld, 2002).

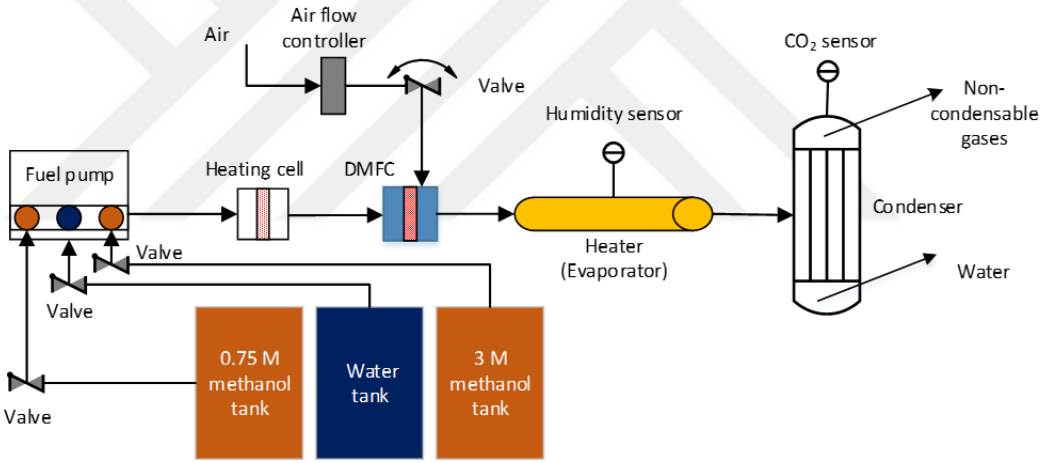

Figure 3.1 The working principles of the experimental setup of DMFC

Using the test station and procedure discussed above, the cell voltages can be measured with an error of less than 1 mV. Deviations in methanol concentration, temperature, and current density lead to higher errors in cell voltage (Engl, 2016). Methanol concentration can be controlled to ± 0.05 mole·L^{-1}, which results in a margin of error in the cell voltage of ± 2 mV. The temperature can be controlled to ± 1°C, resulting in a cell voltage error of ± 5 mV and the current density can be controlled to ± 0.3%, resulting in a cell voltage error of ± 1 mV. A total uncertainty of ± 8 mV can, therefore, be assumed. In a previous publication (Müller et al., 2014), some of the co-authors of the current paper analysed 8 MEAs of the same type used in this publication,

to study degradation under different conditions. Re-analysing the data of the starting measurements before degradation, the standard-deviation in cell voltage is 3 mV to 5 mV, depending on the operating conditions. Thus, the reproducibility is actually better than in the worst-case scenario discussed above. The standard deviation for methanol permeation is 0.002 $A \cdot cm^{-2}$, and standard deviation for water permeation is 0.02 $g \cdot cm^{2} \cdot h^{-1}$.

3.2.1 Results of Experiment of DMFC in cell level

The effects of methanol concentration (0.5, 0.75 and 1M) and flow rate of air (20 and 30 $mL \cdot cm^{-2} \cdot min^{-1}$) on the polarization curve and water and methanol crossover current density were studied. The air flow rate entering the cathode is an important factor in DMFC systems, as oxygen is required for the oxygen reduction reaction (ORR) and it prevents flooding by removing liquid water from the gas diffusion layer and channels (Ge & Liu, 2005). Similarly, methanol concentration has an important effect on cell performance due to the fact that it has a strong influence on the mass transportability of the cell (Colpan et al., 2017). Figure 3.2 illustrates the cell voltage at different air flow rates and methanol concentrations. As discussed in some studies in the literature (Ge & Liu, 2005; Calabriso et al., 2017; Albani & Borello, 2018) a higher air flow rate ensures the transportation of the required oxygen concentration in the cell and improves the ORR activity. The results obtained in this study were in the same trend as the findings of the studies found in the literature. For example, the values of the cell voltage at 0.20 $A \cdot cm^{-2}$ and 0.5 M methanol concentration were 0.366 V and 0.358 V, respectively, for the air flow rates of 30 $mL \cdot cm^{-2} \cdot min^{-1}$ and 20 $mL \cdot cm^{-2} \cdot min^{-1}$. On the other hand, methanol concentration is more influential on the performance of a DMFC. Colpan et al., (2017) showed that lower methanol concentrations and higher current densities ensure low methanol crossover rates due to the increased consumption of methanol and low methanol concentrations at the anode catalyst layer. In addition, at high methanol concentrations and current density, voltage losses increase due to the increased activation and ohmic polarizations. The results for the voltage output (Figure 3.2) and methanol crossover current density (Figure 3.3) show that when the methanol concentrations are 0.5 M, 0.75 M, 1 M and 1.25 M, the voltage

and methanol crossover current density values are found to be 0.360 V (0.011 A·cm^{-2}), 0.391 V (0.035 A·cm^{-2}), 0.390 V (0.067 A·cm^{-2}), and 0.383 V (0.096 A·cm^{-2}), respectively at 0.2 A·cm^{-2} and 30 mL·cm^{-2}·min^{-1}. This means that better cell performances are obtained at 0.75 M and 1 M; while lower performances are seen at 0.5 M and 1.25 M mainly due to the mass transport limitation at the anode and negative effect of methanol crossover, respectively.

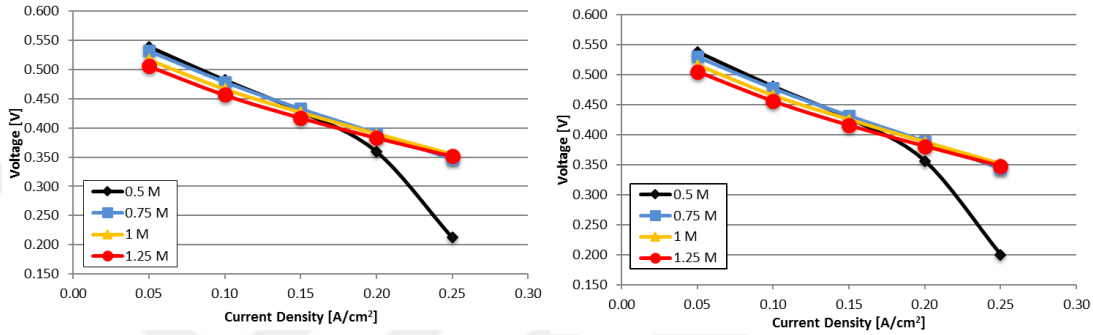

Figure 3.2 Experimentally-obtained DMFC polarization curves at 0.5 M, 0.75 M, 1 M and 1.25 M methanol concentrations and air flow rates of a) 30 mL·cm^{-2}·min^{-1}; b) 20 mL·cm^{-2}·min^{-1}

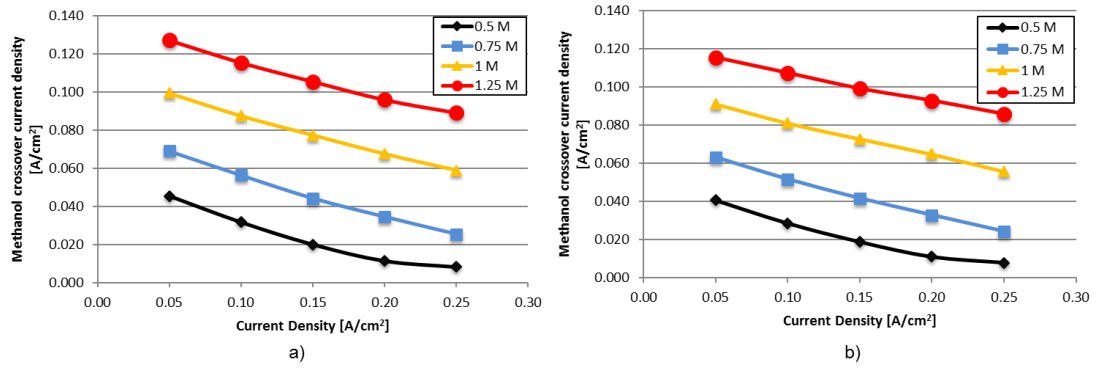

Figure 3.3 Effect of methanol concentrations (0.5, 0.75, 1 and 1.25 M) and air flow rates of: a) 30 mL·cm^{-2}·min^{-1}; b) 20 mL·cm^{-2}·min^{-1} on the methanol crossover current density

Figure 3.4 shows the effect of the methanol concentration, current density and air flow rate on the water crossover. Water permeation is managed by three different mechanisms, namely diffusion, electro-osmosis, and hydraulic permeation (Lu, Liu, et al., 2004; Xu & Zhao, 2007). Hydraulic permeation occurs when there are high-pressure differences between the anode and cathode. C. Xu & Zhao (2007) observed

that the effect of methanol concentration on the water crossover is small. They showed that an increase in the air flow rate leads to an increase in the water crossover due to lower water pressure and higher water fraction in the gas diffusion layer. As is shown in Figure 3.4, the water crossover increases with increasing current density, as expected. The water crossover rate is found to be 0.54 $g \cdot cm^{-2} \cdot h^{-1}$ (for an air flow rate of 30 $mL \cdot cm^{-2} \cdot min^{-1}$) and 0.50 $g \cdot cm^{-2} \cdot h^{-1}$ (for an air flow rate of 20 $mL \cdot cm^{-2} \cdot min^{-1}$) at a current density and methanol concentration of 0.20 $A \cdot cm^{-2}$ and 0.5 M, respectively.

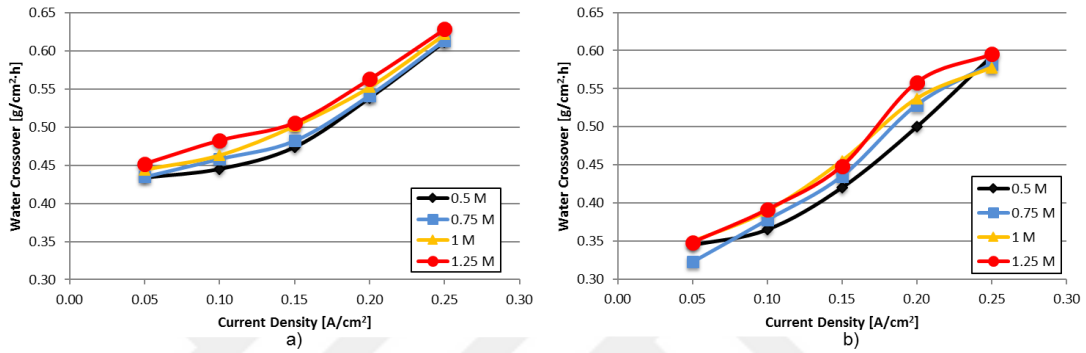

Figure 3.4 Effect of methanol concentrations (0.5, 0.75, 1 and 1.25 M) and air flow rates of: a) 30 $mL \cdot cm^{-2} \cdot min^{-1}$; and b) 20 $mL \cdot cm^{-2} \cdot min^{-1}$ on the water crossover

3.3 Experiment of DMFC in Stack Level

In Forschungszentrum Jülich, a short stack consisting of 5 cells, is measured by short stack test rig for a DMFC. The test rig control uses current density, methanol permeation and air flow rate as input parameters. Temperature and methanol concentration are obtained as output parameters. The input methanol permeation is initially not the real permeation. If the real permeation is, for example, higher, more methanol is consumed in the stack than added by the methanol pump, so methanol concentration and therefore also methanol permeation will decrease, until an equilibrium is reached and the real permeation is equal to the input permeation. Temperature control is done by controlling the thermostat, so that the methanol solution entering the stack has the same temperature then the methanol solution leaving the stack. Thus, thermal losses of the mixing vessel and tubes are compensated for. Thermal losses of the stack are reduced by insulation, but small losses still have to be taken into account. It can be assumed that the first and the last cell lose some heat over

the end plates and are therefore a little cooler than the cells in the middle. The temperature of the stack is mainly defined by electrochemical losses (methanol permeation and cell voltage lower than the voltage defined by the lower heating value of methanol) heating the stack and evaporation of water at the cathode cooling the stack until an equilibrium is reached.

Experiments are performed various current densities (i), methanol permeations (i_{perm}) and AFR as the input parameter. According to the methanol permeation input in the experiment, methanol concentration can be measured as a function of methanol permeation. It also means that the concentrated methanol is refilled into the anode mixing vessel according to the current density and the methanol permeation. After a few hours (generally 1-3 hours) a constant concentration is established and can be measured. The schematic of the experimental system for short stack test rig is illustrated in the Figure 3.5. Methanol-water solution is fed into the anode side of the DMFC from a mixing vessel. Methanol is pumped to the mixing vessel and its flow rate is controlled by a methanol pump. The short stack testing system is controlled by a computer to control the test parameters. A load unit consumes the current generated in the stack, a data-logger reads the response of the DMFC, a mass flow controller (CFC) controls the air flow to the cathode, a refractometer measures methanol concentration and a thermostat heats the methanol solution to the temperature of the methanol outlet to compensate for heat loss in the anode mixing vessel and tubes. Additionally, temperatures are measured by thermometers in anode inlet, anode outlet and cathode outlet.

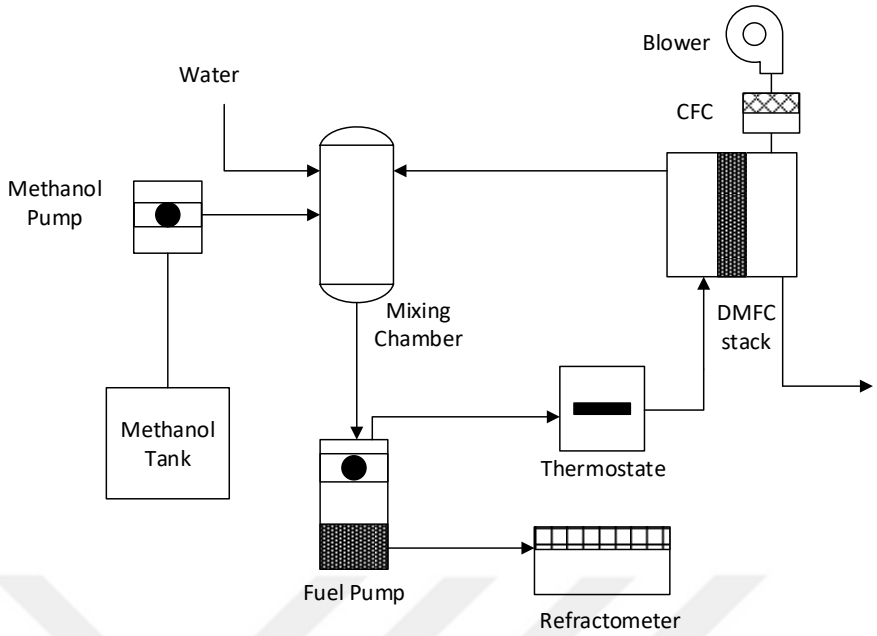

Figure 3.5 Short stack test system for DMFC

The DMFC short stack consists of five cells with 315 cm^2 active area which have Johnson Matthey membrane electrode assemblies (MEA). In the first step of the test procedure, the stack is heated up by heating the anode inlet to 70°C for 1 h (anode inlet temperature symbolized with T_A) with 0.22 $mL \cdot cm^{-2} \cdot min^{-1}$ anode flow rate (V_A), 10 $ml \cdot cm^{-2} \cdot min^{-1}$ air flow rate (V_C), 0.075 $A \cdot cm^{-2}$ permeation current density (i_{perm}) and zero current density. Then, the experiments are performed with three current densities (i) as 0.1, 0.15 and 0.2 $A \cdot cm^{-2}$ and three permeation current densities (i_{perm}) as 0.05, 0.01 and 0.15 $A \cdot cm^{-2}$ individually for various cathode flow rates changed between 10 and 30 $mL \cdot cm^{-2} \cdot min^{-1}$. Each operating step is maintained for 3 hours to reach equilibrium. In order to remove reversible degradation operation is interrupted for 28 seconds after 1800 s of operation (Knights, Colbow, St-Pierre, & Wilkinson, 2004). The interruption consists of three phases for 3, 15 and 10 s with V_{Ci}, 0 and 35 $ml \cdot cm^{-2} \cdot min^{-1}$ cathode flow rate inputs, respectively. At the end of testing there is a 2 h (7200 s) cooing step down to 35 °C operating temperature with 0.22 $mL \cdot cm^{-2} \cdot min^{-1}$ anode flow rate (V_A) and 10 $mL \cdot cm^{-2} \cdot min^{-1}$ cathode flow rate (V_C), 0.075 $A \cdot cm^{-2}$ permeation current density (i_{perm}) and zero current density.

3.3.1 Results of Experiment of DMFC in Stack Level

Short stack test results for average cell voltage are shown in Figure 3.6 for the set values of 50 $mA \cdot cm^{-2}$ 100 $mA \cdot cm^{-2}$ and 150 $mA \cdot cm^{-2}$ permeation current density (i_{perm}). Short stack test procedure was arranged for 0.1 $A \cdot cm^{-2}$, 0.15 $A \cdot cm^{-2}$ and 0.2 $A \cdot cm^{-2}$ current densities (i) so their operating locations are marked in Figure 3.6. Additionally, each location includes three AFR (V_C) of 15, 12 and 10 $mL \cdot cm^{-2} \cdot min^{-1}$, respectively in Figure 3.6-a; 30, 25 and 20 $mL \cdot cm^{-2} \cdot min^{-1}$ respectively in Figure 3.6-b which were detailed in Table 3.1. According to the Figure 3.6-a, average voltage is higher at 50 $mA \cdot cm^{-2}$ permeation current density for 0.1 $A \cdot cm^{-2}$ current density however, better results are shown at 100 $mA \cdot cm^{-2}$ permeation current density for 0.2 $A \cdot cm^{-2}$ current density and 10 $mL \cdot cm^{-2} \cdot min^{-1}$ AFR. Operation of the short stack was not possible at some operating conditions and no average voltage could be obtained. This is due to an air flow rate, which was not sufficient to generate a high current density and oxidize a large amount of permeated methanol at the cathode at the same time. Reliable operation is not achieved for 0.15 $A \cdot cm^{-2}$ – 10 $mL \cdot (min^{-1} \cdot cm^{-2})$ AFR, for 0.2 $A \cdot cm^{-2}$ – 10, 12 $mL \cdot cm^{-2} \cdot min^{-1}$ AFR at 150 i_{perm} and for 0.2 $A \cdot cm^{-2}$ – 10 $mL \cdot cm^{-2} \cdot min^{-1}$ AFR at 50 and 100 i_{perm}. However, the failure is not observed for higher AFR average cell voltage of the stack and the results shows more regular characteristics in Figure 3.6-b.

In Figure 3.6-b, better results are observed at 100 $mA \cdot cm^{-2}$ permeation current density for all current densities and average voltage increases about 0.1 V when AFR changes from the higher value to the lower at each current density. For example, average cell voltage yields 0.36 V for 30 $mL \cdot cm^{-2} \cdot min^{-1}$ AFR, 0.37 V for 25 $mL \cdot cm^{-2} \cdot min^{-1}$ AFR and 0.38 V for 20 $mL \cdot cm^{-2} \cdot min^{-1}$ AFR. For general evaluation, it can be expressed that better average cell voltage could be achieved from the stack by lower AFR just for lower current densities but using higher AFR offers reliable operation despite the lower voltage.

Table 3.1 Input parameters of the short stack test, n/a means that this parameter is a measured output parameter in this operating phase

Purpose	Number of repeat	t	i	V_A	V_C	I_{perm}	T_A	ΔT
Heating	1	3600	0	0.22	10	0.075	70	n/a
for each V_{Ci} of 10-12-15-20-25-30	6	1800	0.1	0.3	V_{Ci}	0.05	n/a	0
		3	0	0.3	V_{Ci}	0.05	n/a	0
		15	0	0.3	0	0.05	n/a	0
		10	0	0.3	35	0.05	n/a	0
for each V_{Ci} of 10-12-15-20-25-30	6	1800	0.15	0.3	V_{Ci}	0.05	n/a	0
		3	0	0.3	V_{Ci}	0.05	n/a	0
		15	0	0.3	0	0.05	n/a	0
		10	0	0.3	35	0.05	n/a	0
for each V_{Ci} of 10-12-15-20-25-30	6	1800	0.2	0.3	V_{Ci}	0.05	n/a	0
		3	0	0.3	V_{Ci}	0.05	n/a	0
		15	0	0.3	0	0.05	n/a	0
		10	0	0.3	35	0.05	n/a	0
for each V_{Ci} of 10-12-15-20-25-30	6	1800	0.1	0.3	V_{Ci}	0.1	n/a	0
		3	0	0.3	V_{Ci}	0.1	n/a	0
		15	0	0.3	0	0.1	n/a	0
		10	0	0.3	35	0.1	n/a	0
for each V_{Ci} of 10-12-15-20-25-30	6	1800	0.15	0.3	V_{Ci}	0.1	n/a	0
		3	0	0.3	V_{Ci}	0.1	n/a	0
		15	0	0.3	0	0.1	n/a	0
		10	0	0.3	35	0.1	n/a	0
for each V_{Ci} of 10-12-15-20-25-30	6	1800	0.2	0.3	V_{Ci}	0.1	n/a	0
		3	0	0.3	V_{Ci}	0.1	n/a	0
		15	0	0.3	0	0.1	n/a	0
		10	0	0.3	35	0.1	n/a	0
for each V_{Ci} of 10-12-15-20-25-30	6	1800	0.1	0.3	V_{Ci}	0.15	n/a	0
		3	0	0.3	V_{Ci}	0.15	n/a	0
		15	0	0.3	0	0.15	n/a	0
		10	0	0.3	35	0.15	n/a	0
for each V_{Ci} of 10-12-15-20-25-30	6	1800	0.15	0.3	V_{Ci}	0.15	n/a	0
		3	0	0.3	V_{Ci}	0.15	n/a	0
		15	0	0.3	0	0.15	n/a	0
		10	0	0.3	35	0.15	n/a	0
for each V_{Ci} of 10-12-15-20-25-30	6	1800	0.2	0.3	V_{Ci}	0.15	n/a	0
		3	0	0.3	V_{Ci}	0.15	n/a	0
		15	0	0.3	0	0.15	n/a	0
		10	0	0.3	35	0.15	n/a	0
Cooling	1	7200	0	0.22	10	0.075	35	n/a

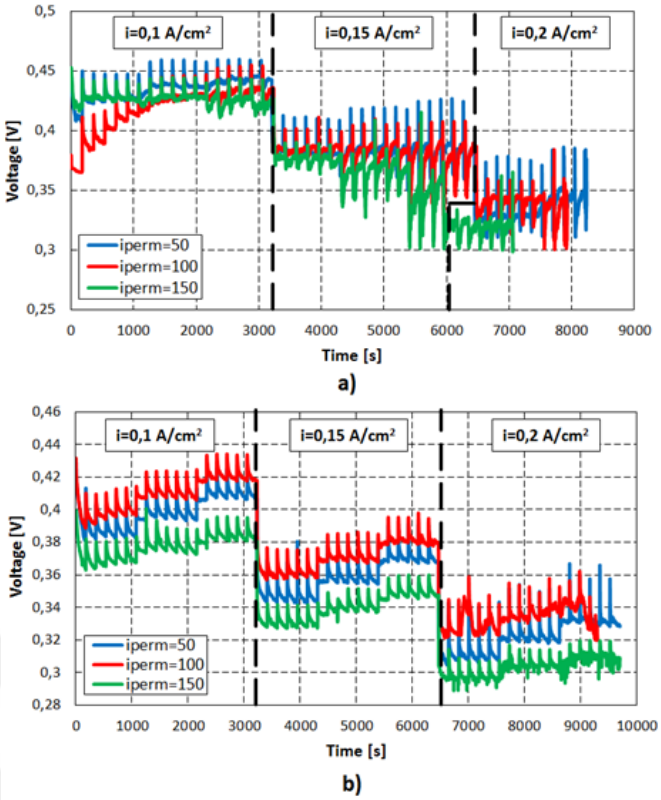

Figure 3.6 Test results of short stack for average cell voltage at 0.1 A·cm^{-2}, 0.15 A·cm^{-2} and 0.2 A·cm^{-2} current density and (a) lower CFR (15, 12, 10 mL·cm^{-2}·min^{-1}) and (b) higher CFR (30, 25, 20 mL·cm^{-2}·min^{-1})

3.4 Comparisons between testing results for single cell and the stack

In this part, a comparative study which includes single cell testing and short stack testing, of a DMFC is presented. Voltage results at various cathode air flow rates, temperatures, methanol concentrations and methanol permeations are compared. As a result, we are able to show the strengths and weaknesses of each of the two methods for DMFC characterization.

Although the single cell test conditions are arranged according to the short stack results for the comparison, the results from the single cell test rig is taken for three methanol concentrations (0.5 M, 1 M and 1.5 M) and three AFR (10, 20 and 30 mL·cm^{-2}·min^{-1}) to investigate the performance characteristics of single cell. The results are shown in the Figure 3.7 for 70 °C operating temperature. Although a higher voltage can be observed at lower current densities at 0.5 M methanol concentration, cell

voltage drops increasingly after the 0.15 $A \cdot cm^{-2}$ current density at all AFR inputs. It is shown that the effect of AFR on cell voltage is small in the entire current density range. Highest outputs are achieved between 0.55 V and 0.45 V at current densities below 0.15 $A \cdot cm^{-2}$ with 0.5 M concentration and between 0.45 V and 0.36 V at current densities above 0.15 $A \cdot cm^{-2}$ with 1 M concentration. It is expected that higher voltages could be obtained for current densities higher than 0.25 $A \cdot cm^{-2}$ with 1.5 M methanol concentration if higher current densities were investigated in single cell tests. But, the range between 0.05 $A \cdot cm^{-2}$ and 0.25 $A \cdot cm^{-2}$ is considered sufficient to compare with the average cell voltage results on short stack.

A comparison of the cell voltage from single cell testing and the cell voltage of each cell in the short stack are presented in Figure 3.7 as a function of methanol concentration. Additionally, the operating parameters temperature, methanol permeation and AFR are shown in the graphics at the right side. The same operating points are represented with two graphics in which one of them shows voltage results and the other shows the input parameters for the same current density. Voltage results are shown in Figure 3.7-a for 0.1 $A \cdot cm^{-2}$, in Figure 3.7-b for 0.15 $A \cdot cm^{-2}$ and in Figure 3.7-c for 0.2 $A \cdot cm^{-2}$ current density. Requested operating parameters which were arranged according to short stack test results, were defined in the single cell testing. However, comparison results which is presented in Figure 3.7, does not comprise all outputs for each inputs because of the failures in single cell testing at lower temperatures.

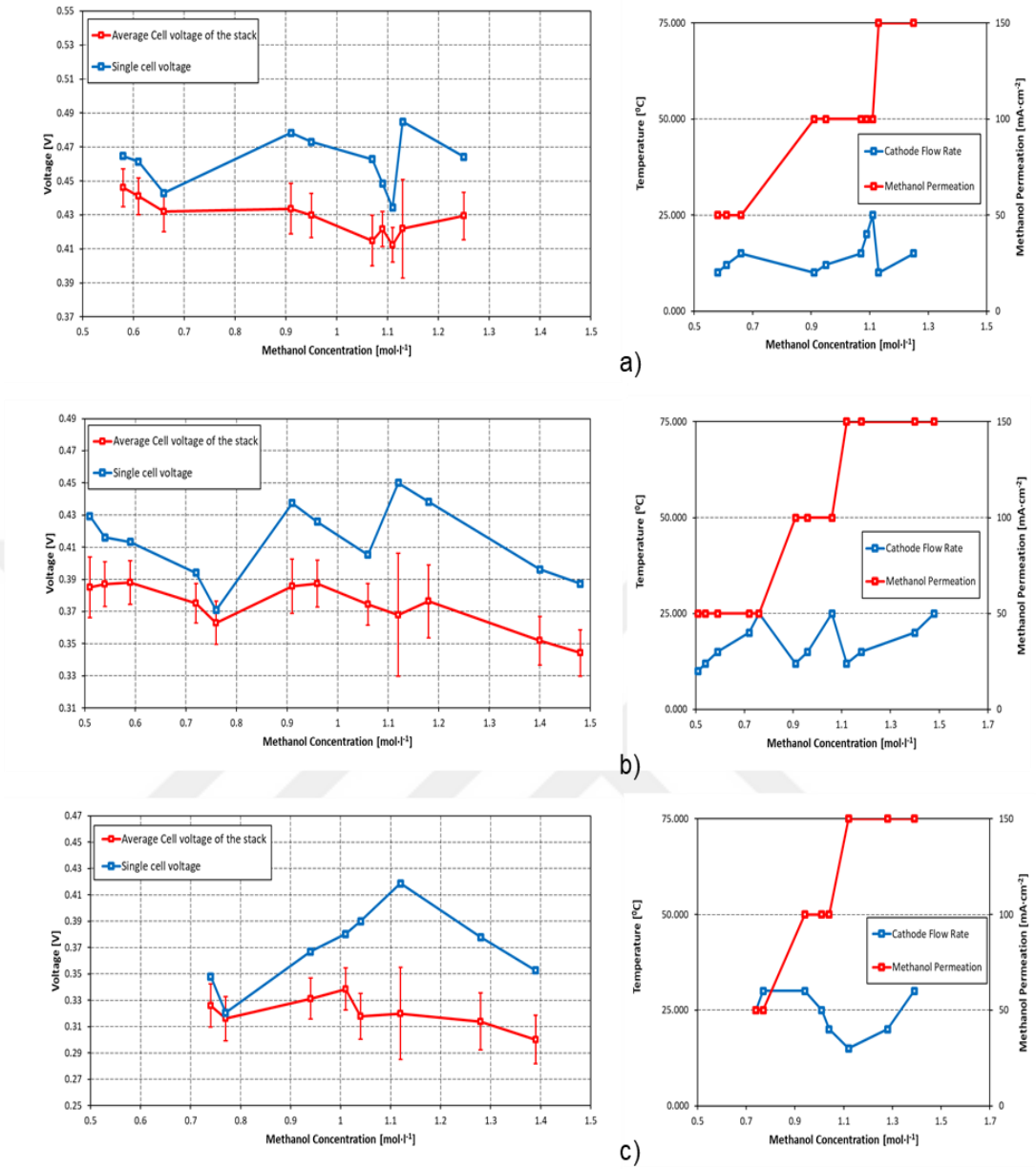

Figure 3.7 Voltage result comparison between single cell test and each cell from short stack test in 0.1 $A \cdot cm^{-2}$ (a), 0.15 $A \cdot cm^{-2}$ (b), 0.2 $A \cdot cm^{-2}$ (c) for various methanol concentrations and other operation parameters of T_A, C_{MeOH} and AFR (right graphs)

CHAPTER FOUR
SYSTEM ANALYSIS

4.1 System Description

The DMFC system requires some auxiliary equipment (a methanol tank, mixing chamber, condenser, filter, blower, and pumps) to feed diluted methanol solution and air to the anode and cathode sides, respectively, at the desired values and to manage heat. A schematic of the DMFC system is shown in Figure 4.1. In this system, a methanol solution at the desired concentration is obtained by mixing pure methanol and liquid water from the anode and cathode outlets. This methanol solution is fed to the anode side of the DMFC by a fuel pump (State 3); while air, which is mainly composed of nitrogen (N_2), O_2 and H_2O_v, is sent to the cathode side after passing through an air blower and filter (State 5).

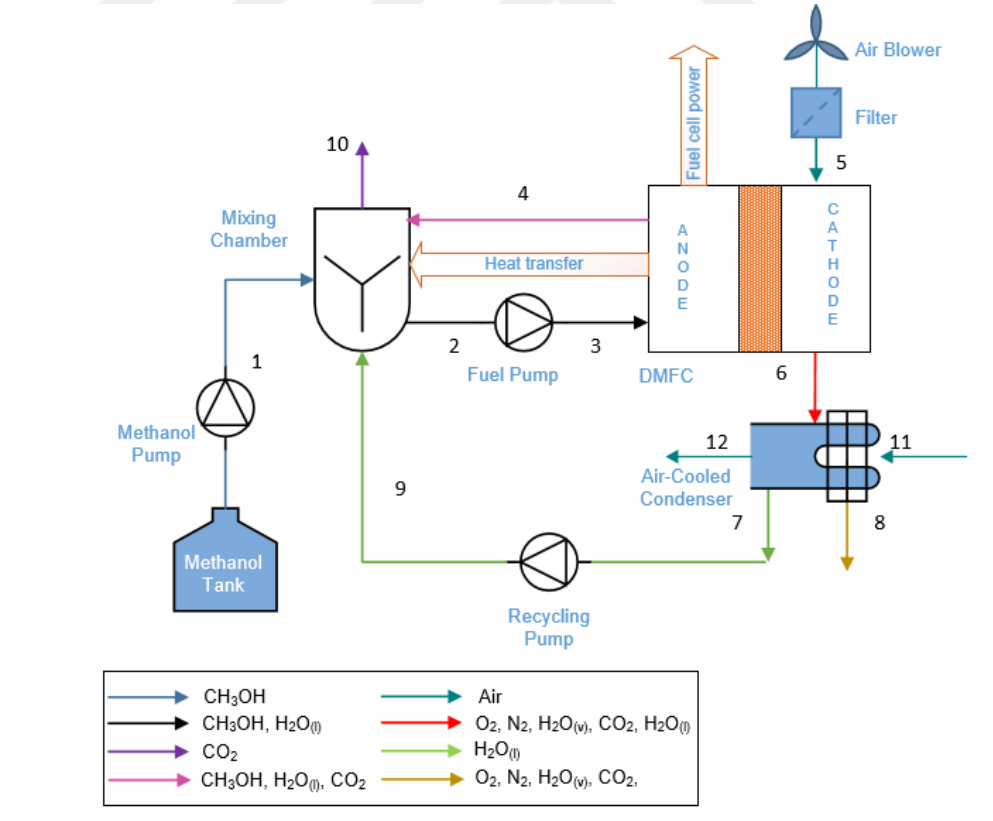

Figure 4.1 Schematic of the DMFC system

In the DMFC, in addition to the generated power, carbon dioxide (CO_2) and water are produced at the anode side, whereas part of the O_2 and water is consumed at the cathode side as a result of the reactions shown in Eqs. (4.1) and (4.2). A portion of methanol permeates (CH_3OH_{perm}) to the cathode, mainly owing to the diffusion of methanol through the membrane; and CO_2 and water are formed at the cathode as shown in Eq. (4.3) (Dohle et al., 2002). Similarly, a portion of water permeates to the cathode due to electro-osmosis, hydraulic permeation, and diffusion (Lu et al., 2005). Excess methanol and water leaving the anode side enter the mixing chamber, together with CO_2 generated at the anode (State 4). CO_2 is then released into the atmosphere from the top of this chamber (State 10). On the other hand, two-phase water and dry gas composed of CO_2, O_2 and N_2 leave the cathode side of the DMFC (State 6). This stream is then cooled passing through the condenser. Here, some of the water vapor converts into liquid water according to the system's water requirement and the liquid water returns to the mixing chamber via the recycling pump (State 7). Unused gases are emitted to the atmosphere (State 8).

$$\text{Anode: } CH_3OH + H_2O \rightarrow CO_2 + 6H^+ + 6e^- \quad (4.1)$$

$$\text{Cathode: } 1.5O_2 + 6H^+ + 6e^- \rightarrow 3H_2O \quad (4.2)$$

$$\text{Cathode: } CH_3OH_{perm} + 1.5O_2 \rightarrow CO_2 + 2H_2O \quad (4.3)$$

4.2 Thermodynamic Modelling of DMFC System

4.2.1 Mass and Energy Analysis

In the system-level mathematical model, data obtained from the DMFC experiments such as methanol crossover current density (i_{perm}), water crossover rate ($\dot{m}''H_2O_{perm}$) and cell voltage (V), as given in Chapter 3, are implemented in the thermodynamic model of the DMFC system. These data are first represented in polynomial-form equations using the curve-fitting method. These equations are then coupled to the modeling equations of the DMFC to find the mass flux at the inlet and outlet of the anode and cathode sides, and the heat loss and power density of the

DMFC. Mass and energy balances are then applied around the control volumes enclosing the BOP components to find the thermodynamic properties of each state and heat and work interactions between the system and its surroundings. This model gives the electrical efficiency, power consumption of auxiliary equipment, net power output and condenser outlet temperature as the output parameters. The main input parameters for this model are shown in Table 4.1. The main assumptions used in this model are listed below:

- The system operates under steady-state conditions.
- All the gases are treated as an ideal gas, whereas liquids are considered as incompressible fluids.
- The kinetic and potential energy are neglected.
- Methanol crossed over to the cathode reacts with O_2 to form CO_2 and H_2O.
- The evaporation of methanol and water is negligible, except at the cathode.
- Heat losses from the auxiliary equipment are neglected.
- The temperature of the cell inlet and outlet are the same and equal to the operating temperature.

Table 4.1 Main input data used for the baseline simulation

Parameters	**Value**
Anode flow rate (States 2 and 3)	0.23 $mL \cdot cm^{-2} \cdot min^{-1}$
Faraday constant	96485 $s \cdot A \cdot mol^{-1}$
Isentropic efficiency	0.6
Temperature of cell	70 °C
Pressure of ambient air	100 kPa
Temperature of ambient air	25 °C
Relative humidity ratio of ambient air	0.10
Relative humidity ratio of condenser inlet	1 (Assumed)
Relative humidity ratio of condenser outlet	1 (Assumed)

Methanol is consumed in the electro-chemical reaction (Eq. (4.1)) and also permeates from the anode to the cathode (Eq. (4.3)). The total methanol consumption rate can be calculated as follows:

$$\dot{m}''_{CH_3OH,cons} = \frac{(i+i_{perm})}{6 \cdot F} \cdot MW_{CH_3OH} \cdot 3.6 \qquad (4.4)$$

Here, 3.6 is the unit conversion factor (from $g \cdot s^{-1} \cdot cm^{-2}$ to $kg \cdot h^{-1} \cdot cm^{-2}$).

In a galvanic process, the stoichiometry ratio (λ) is defined as the ratio of supplied mass flux to the required mass flux for the reaction (Karaoğlan et al., 2018). The stoichiometric ratio of the anode (λ_a) is a parameter used to find the total flow rate of the methanol fed to the anode side of the DMFC stack. If a mass balance is applied to the mixing chamber for methanol, the flow rate of pure methanol leaving the methanol tank can be found. Hence, the mass flux of methanol entering and leaving the anode side and leaving the methanol tank can be shown with their state numbers, respectively, as follows:

$$\dot{m}''_{2,CH_3OH} = \dot{m}''_{CH_3OH,cons} \cdot \lambda_a \tag{4.5}$$

$$\dot{m}''_{4,CH_3OH} = \dot{m}''_{CH_3OH,cons} \cdot (\lambda_a - 1) \tag{4.6}$$

$$\dot{m}''_{1,CH_3OH} = \dot{m}''_{2,CH_3OH} - \dot{m}''_{4,CH_3OH} \tag{4.7}$$

The mass flux of water entering the anode can be determined depending on the concentration of methanol, methanol mass flux, densities and molecular weights of methanol and water at the anode inlet as follows:

$$\dot{m}''_{2,H_2O} = \dot{m}''_{2,CH_3OH} \cdot \frac{\rho_{H_2O}}{MW_{H_2O}} \cdot \left(\frac{1}{C_{MeOH}} - \frac{MW_{CH_3OH}}{\rho_{CH_3OH}} \right) \tag{4.8}$$

The mass flux of water consumed due to the electrochemical reactions at the anode is primarily a function of the current density and can be calculated as:

$$\dot{m}''_{H_2O,cons} = \frac{i}{6 \cdot F} \cdot MW_{H_2O} \cdot 3.6 \tag{4.9}$$

The mass flux of water and CO_2 leaving the DMFC (State 4) can be found using Eqs. (4.10) and (4.11), respectively:

$$\dot{m}''_{4,H_2O} = \dot{m}''_{2,H_2O} - \left(\dot{m}''_{H_2O,cons} + \dot{m}''_{H_2O,perm} \right) \tag{4.10}$$

$$\dot{m}''_{4,CO_2} = \frac{i}{6 \cdot F} \cdot MW_{CO_2} \cdot 3.6 \tag{4.11}$$

When the mass balance for water is applied to the mixing chamber, the mass flux of required water that must be recycled ($\dot{m}''_{7,H_2O}$) from the condenser can be written as:

$$\dot{m}''_{7,H_2O} = \dot{m}''_{2,H_2O} - \dot{m}''_{4,H_2O}$$
$$= \dot{m}''_{H_2O,cons} + \dot{m}''_{H_2O,perm} \quad (4.12)$$

Water is generated at the cathode by the reacted and crossed over methanol (Jiang and Chu, 2008). The total mass flux of generated water can be calculated using Eq. (4.13). Here, the first and second terms in parentheses give the water production due to ORR and the methanol oxidation reaction (MOR) on a mole basis, respectively.

$$\dot{m}''_{H_2O,gen} = \left(\frac{i}{2\cdot F} + \frac{i_{perm}}{3\cdot F}\right) \cdot MW_{H_2O} \cdot 3.6 \quad (4.13)$$

Air, which is composed of H_2O_v, N_2, CO_2, and O_2, is fed to the cathode inlet with a cathodic stoichiometric ratio (λ_c) that is greater than 1 (Li & Faghri, 2013). Oxygen is consumed due to the oxygen reduction reaction (Eq. (4.2)) and the reaction of permeated methanol with O_2 (Eq. (4.3)). The mass flux of constituents found in the air entering the cathode can be found as shown in Eqs. (4.14)-(4.16), respectively. 0.622 is the ratio of molecular weight of water vapor to that of air. Note that the mass flux of CO_2 in the air is considered to be negligible in this study.

$$\dot{m}''_{5,O_2} = \frac{(i+i_{perm})}{4\cdot F} \cdot \lambda_c \cdot \sum(x_k \cdot MW_k) \cdot 3.6 \cdot \frac{1}{x_{O_2}} \quad (4.14)$$

$$\dot{m}''_{5,N_2} = \frac{(i+i_{perm})}{4\cdot F} \cdot \lambda_c \cdot \sum(x_k \cdot MW_k) \cdot 3.6 \cdot \frac{1}{x_{N_2}} \quad (4.15)$$

$$\dot{m}''_{5,H_2O_{(v)}} = \frac{(i+i_{perm})}{4\cdot F} \cdot \lambda_c \cdot \sum(x_k \cdot MW_k) \cdot 0.622 \cdot \frac{P_5,sat,H_2O_{(v)}\cdot\varphi_{c,i}}{(P_{total}-P_5,sat,H_2O_{(v)}\cdot\varphi_{c,i})} \cdot 3.6 \quad (4.16)$$

As a result of the cathodic reactions, CO_2 is produced (Eq. (4.17)), and O_2 is consumed. While the flow rate of O_2 leaving cathode is equal to the oxygen flow rate

entering the cathode minus the consumed flow rate of O_2, the mass flow rate of N_2 remains constant through the cell and condenser. H_2O_v also forms at the cathode because of evaporation (Eq. (4.18)) (Jiang & Chu, 2008). Hence, the gas mixture leaving the cathode consists of O_2, CO_2, N_2, and $H_2O_{(v)}$. The equations that give the mass flux of the gas mixture and liquid water at the cathode outlet are given in Eqs. (4.19) and (4.20):

$$\dot{m}''_{6,CO_2} = \frac{(i+i_{perm})}{4 \cdot F} \cdot MW_{O_2} \cdot 3.6 \tag{4.17}$$

$$\dot{m}''_{6,H_2O_{(v)}} = \dot{m}''_{6,\text{total gas}} \cdot \left(0.622 \cdot \frac{P_6,sat,H_2O_{(v)} \cdot \varphi_{c,o}}{(P_{total} - P_6,sat,H_2O_{(v)} \cdot \varphi_{c,o})}\right) \tag{4.18}$$

$$\dot{m}''_{6,\text{total gas}} = \dot{m}''_{6,O_2} + \dot{m}''_{6,N_2} + \dot{m}''_{6,CO_2} + \dot{m}''_{6,H_2O_{(v)}} \tag{4.19}$$

$$\begin{aligned}\dot{m}''_{6,H_2O_{(l)}} = {} & \dot{m}''_{H_2O,gen_{ec}} + \dot{m}''_{H_2O,gen_{mc}} \\ & + \dot{m}''_{H_2O,perm} + \dot{m}''_{5,H_2O_{(v)}} - \dot{m}''_{6,H_2O_{(v)}}\end{aligned} \tag{4.20}$$

It is assumed that the gas mixture enters and leaves the condenser fully saturated and so the relative humidity is considered 100% at the states (Izenson & Hill, 2005; Schultze & Horn, 2012). The dry (non-condensable) gases and H_2O_v are then cooled down in the condenser. While a large part of water vapor condenses, the other part of the water vapor and dry gas are released to the atmosphere (State 8). The mass balance for the condenser is given in Eq. (4.21). Here, H_2O_v depends on the saturated pressure, relative humidity and total mass flux of the condenser outlet (Eq. (4.22)), which is the sum of the mass fluxes of total dry gas and H_2O_v (Eq. (4.23)).

$$\dot{m}''_{8,H_2O_{(v)}} = \dot{m}''_{6,H_2O_{(v)}} + \dot{m}''_{6,H_2O_{(l)}} - \dot{m}''_{7,H_2O} \tag{4.21}$$

$$\dot{m}''_{8,H_2O_{(v)}} = \dot{m}''_{8,\text{total gas}} \cdot \left(0.622 \cdot \frac{P_8,sat,H_2O_{(v)} \cdot \varphi_{cond,e}}{(P_{total} - P_8,sat,H_2O_{(v)} \cdot \varphi_{cond,e})}\right) \tag{4.22}$$

$$\dot{m}''_{8,\text{total gas}} = \dot{m}''_{8,\text{drygas}} + \dot{m}''_{8,H_2O_{(v)}} \tag{4.23}$$

The relationship between the condensation temperature and pressure for water is represented with Antoine's equation (Thomson, 1946), as shown below:

$$\ln\left(\frac{P_8,sat,H_2O_{(v)}}{bar}\cdot\varphi_{cond,e}\right)=A-\frac{B}{C+T_{cond}/^{\circ}C} \tag{4.24}$$

Here, A is 11.9648, B is 3984.923, and C is 233.426.

The electrical efficiency of the system can be given as the ratio of net power output of the system to the lower heating value (LHV) of the methanol (28.6×106 kJ·m^{-3}) leaving the fuel tank. As water is removed from the cell mostly in the gaseous phase as a result of the reactions, LHV is used in the calculation of the electrical efficiency (Eq. (4.25)) (Andrian & Meusinger, 2000). The net power density of the system [W·cm^{-2}] can be found by subtracting the power density of the fuel cell from the total power density consumption of the auxiliary components (blower, fuel pump, methanol pump, and recycling pump), as shown in the numerator of the right-hand side of Eq. (4.26).

$$\eta_{electrical_{system}}=\frac{i\cdot V-\sum W''_{aux,j}}{\dot{m}''_{1,CH_3OH}\cdot LHV_{CH_3OH}\cdot v_{1,CH_3OH}}\cdot\frac{1}{3.6} \tag{4.25}$$

$$\sum W''_{aux\,j}=\sum\left(\frac{\dot{m}''\cdot\Delta P\cdot v}{\eta\cdot3.6}\right)_j \tag{4.26}$$

In Eq. (4.26), ΔP denotes the pressure drop in the jth auxiliary equipment. For this system, the pressure drops in the cell and condenser are taken as 200 Pa and 300 Pa, respectively (Karaoğlan et al., 2018; Nölke, 2007). In addition, the pressure drop in the mixing chamber is neglected.

In DMFC systems, as the mixing chamber and DMFC are generally located very close to each other (Janssen et al., 2010), it may be considered that there is a heat transfer between the DMFC and the mixing chamber. It can be assumed that the heat loss rate from the DMFC $\left(\dot{Q}''_{FC}\right)$ is equal to the heat demand of the mixing chamber $\left(\dot{Q}''_{MXC}\right)$, if all the other components are considered as well-insulated. The steady-state energy balance around the control volumes enclosing the DMFC and the mixing chamber are given in Eqs. (4.27) and (4.28), respectively.

$$\dot{Q}''_{FC} = W''_{FC} + \frac{1}{3.6} \cdot \left(\sum(\dot{m}'' \cdot h)_o - \sum(\dot{m}'' \cdot h)_i \right) \quad (4.27)$$

$$\dot{Q}''_{MXC} = \frac{1}{3.6} \cdot \left(\sum(\dot{m}'' \cdot h)_o - \sum(\dot{m}'' \cdot h)_i \right) \quad (4.28)$$

In Eqs. (4.27) and (4.28), h represents the specific enthalpy, which is the summation of enthalpy of formation and the change of enthalpy between the given state and the reference state (Mench, 2008). The thermodynamic data were obtained using the EES library.

4.2.2 Exergy Analysis

In this chapter, the modeling equations of exergy analysis for this system is presented. Exergy is defined as the maximum work that may be achieved by bringing a system into equilibrium (mechanical, thermal and chemical) with its environment (Colpan, 2012). Exergy analysis is a useful tool that can be used to find the locations and magnitudes of exergy destructions (a measure of irreversibilities) in the thermodynamic systems. Exergy is destructed due to irreversibilities such as friction, mixing, chemical reaction and heat transfer for DMFC system components. In this analysis, the exergy flow for the chemical species in each state is first calculated. Secondly, the exergy destructions are found using exergy balance applied to enclosing system components. Finally, the performance assessment for DMFC and its system is performed. It should be noted that the exergy analysis, is done in mole basis for this study.

4.2.2.1 Exergy Flows

The total exergy is composed of the thermo-mechanical ($\overline{ex}_i^{TM}$) and the chemical exergy ($\overline{ex}_i^{Ch}$).

$$\overline{ex}_i = \overline{ex}_i^{Th-Me} + \overline{ex}_i^{Ch} \quad (4.29)$$

4.2.2.1.1 Thermo-mechanical Exergy. The thermo-mechanical exergy is defined as the maximum theoretical achievable work when the system brings into mechanical and thermal equilibrium (e.g. temperature and pressure) with the reference of environment. It should be pointed out that we assumed the potential and kinetic energies are negligible in this analysis.

$$\bar{ex}_i^{TM} = \left(\bar{h}_i - \bar{h}_0\right) - T_o \cdot (\bar{s}_i - \bar{s}_0) \tag{4.71}$$

where $\bar{h}$ and $\bar{s}$ represent the specific enthalpy and entropy of species, respectively, and T_o is the temperature of the reference environment. For this study, the reference temperature and pressure are 101.325 kPa and 298.15 K respectively. The enthalpy ($\bar{h}_0$) and entropy ($\bar{s}_0$) values at the reference environment are given in the Table 4.2.

Table 4.2 The reference values of specific enthalpy and entropy at the 298.15 K and 101.325 kPa (Mench, 2008)

Species, j	**Specific Enthalpy, $\bar{h}_0$ (kJ/kmol)**	**Specific Entropy, $\bar{s}_0$ (kJ/kmol-K)**
CH_3OH	- 238,810	126.8
H_2O_v	-241,811	188.7
H_2O_l	-285,830	69.9
CO_2	- 393,520	213.7
O_2	0	205
N_2	0	191.5

4.2.2.1.2 Chemical exergy. The chemical exergy is defined as the maximum theoretical work achievable when the system brings into chemical equilibrium with the reference of environment which is given Table 4.3.

Table 4.3 Molar gas composition of the environment at the dead state (Moran et al., 2010)

Species, j	**x^e (%)**
H_2O	3.12
CO_2	0.03 (Neglected)
O_2	20.35
N_2	75.67

The general calculation of chemical flow exergy for ideal gas is given as follows:

$$\overline{ex}_i^{CH} = \sum X_j \cdot \overline{ex}^{o}{}_j^{CH} + R_u \cdot T_{ref} \cdot \sum X_j \cdot \ln(X_j) \tag{4.72}$$

Liquid water existed in system has chemical exergy because it is found in environment as vapor phase. In this case, the chemical exergy of liquid water is calculated using Eq. (4.73). This equation gives the same results with the value of standard chemical exergy.

$$\overline{ex}_{H_2O}^{CH} = \left[\bar{g}_{H_2O_l} - \bar{g}_{H_2O_g}\right] + R_u \cdot T_o \cdot \ln\left(\frac{1}{X^e{}_{H_2O}}\right) \tag{4.73}$$

Calculating the chemical exergy of methanol substance which is not existed in environment, the methanol is considered that it reacts with other substances known their chemical exergy. In this case, the chemical exergy of methanol is calculated using Eq. (4.74). This equation corresponds to the standard chemical exergy value.

$$\overline{ex}_{CH_3OH}^{CH} = \left[\bar{g}_{CH_3OH_l} - \frac{3}{2}\bar{g}_{O_2} - \bar{g}_{CO_2} - 2\bar{g}_{H_2O_g}\right] + R_u \cdot T_o \cdot \ln\left(\frac{X_{O_2}{}^{e^2}}{X^{e^2}{}_{H_2O_g} \cdot X^e_{CO_2}}\right) \tag{4.74}$$

In these equations, where X_j is the mole fraction of the species j in the system, $\overline{ex}_j^{CH}$ is the chemical exergy of species j in the system at the reference environment. The chemical exergy flows of these species at the reference environment are shown in Table 4.4.

Table 4.4 The chemical exergy values of species at the 298.15 K and 101.325 kPa (Moran et al., 2010)

Species, j	**Standard Chemical Exergy, $\overline{ex}_j^{CH}$ (kJ/kmol)**
H_2O	8,635
CO_2	14,175
CH_3OH	718,000
O_2	3,950
N_2	640

4.2.2.2 Exergy balance

The steady-state exergy balance around the control volumes enclosing the system components is presented in Eqs. (4.75)-(4.78).

$$0 = \sum_j \dot{E}_{Q,j} - \dot{E}x_{W_{cv}} + \sum_i \dot{E}x_i - \sum_o \dot{E}x_o - \dot{E}x_D \tag{4.75}$$

where

$$\dot{E}_{Q,j} = \left(1 - \frac{T_{ref}}{T_j}\right) \cdot Q_j \tag{4.76}$$

$$\dot{E}x_i = \dot{n}_i \cdot \overline{ex}_i \tag{4.77}$$

$$\dot{E}x_o = \dot{n}_o \cdot \overline{ex}_o \tag{4.78}$$

where $\overline{ex}_i$ and $\overline{ex}_o$ are the specific molar exergy ($J \cdot mol^{-1}$) at the input and output species, respectively, and the $\dot{E}x_i$ and $\dot{E}x_o$ are the total exergy flow rate at the input and output, respectively. $\dot{E}x_D$ is defined as the exergy destruction rate in the control volume of the system components. $\dot{E}_{Q,j}$ represents the total exergy transfer by heat, and it is neglected for this calculation. $\dot{E}x_{W_{cv}}$ is the total exergy transfer due to work.

4.2.2.3 Exergetic performance parameters

The exergetic efficiency (second law efficiency) gives better performance assessment of the system in terms of thermodynamic (Kazim, 2004). For this system, the exergetic efficiency is defined as the ratio of net power output to the exergy of the fuel (methanol) entering the system. Therefore, the exergetic efficiency of the system is calculated using Eq. (4.79).

$$\varepsilon_{system} = \frac{\dot{W}_{net\_electrical}}{\dot{n}_{CH_3OH,1} \cdot \overline{ex}_{CH_3OH,1}} \tag{4.79}$$

The exergetic efficiency for DMFC in cell level is also calculated in this study to better understand the operation of DMFC. The exergetic efficiency for DMFC is defined as following:

$$\varepsilon_{cell} = \frac{\dot{W}_{fuelcell}}{\sum(\dot{n}_j \cdot \overline{ex}_j)_i} \tag{4.80}$$

Table 4.5 Control volume and exergy balance equations for each system components

Components	**Control Volume**	**Exergy Balance**
Methanol Pump		$\dot{W}_{P,meth} + \dot{E}x_0 - \dot{E}x_1 - \dot{E}x_{D,p_{meth}} = 0$
Fuel Pump		$\dot{W}_{P,fuel} + \dot{E}x_2 - \dot{E}x_3 - \dot{E}x_{D,P_{fuel}} = 0$
Mixing Chamber	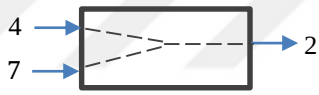	$\dot{E}x_4 + \dot{E}x_7 - \dot{E}x_2 - \dot{E}x_{D,chamber} = 0$
Methanol Tank	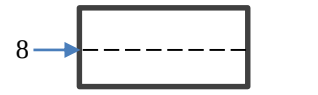	$\dot{E}x_8 - \dot{E}x_{D,tank} = 0$
Recycling Pump	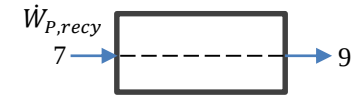	$\dot{E}x_7 - \dot{E}x_9 - \dot{E}x_{D,P_{recy}} = 0$
Blower	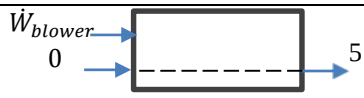	$\dot{E}x_0 + \dot{E}x_5 - \dot{W}_{blower} - \dot{E}x_{D,blower} = 0$
DMFC	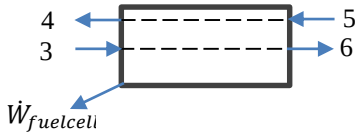	$\dot{E}x_5 + \dot{E}x_3 + \dot{E}x_6 - \dot{E}x_4 - \dot{W}_{fuelcell} - \dot{E}x_{D,fuelcell} = 0$
Condenser	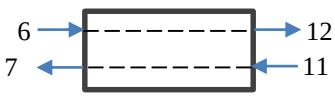	$\dot{E}x_6 + \dot{E}x_{11} - \dot{E}x_{12} - \dot{E}x_7 - \dot{E}x_{D,COND} = 0$

4.3 Water Autonomy Management with Condenser in DMFC system

The condenser found in DMFC systems plays a key role because the saturated mixture flow composed of O_2, CO_2, N_2, and H_2O leaving the DMFC is cooled down, and vapor phase of H_2O is converted to liquid phase through air-cooled condenser which is shown Figure 4.2. In this study, the geometric properties of condenser given in Table 4.6 are taken from the literature (Nölke, 2007). The condenser geometry is shown in Figure 4.3. In addition, the condenser working requirements are obtained from the semi-empirical system model. The calculation algorithm is presented in Table 4.7. Accordingly, after the parameters mentioned above are set in the 3-D model in COMSOL Multiphysics, the continuity and momentum equations given below are solved.

$$\rho(u \cdot \nabla)u = \nabla \cdot [-\rho I + K] + F \tag{4.81}$$

$$\nabla \cdot (\rho u) = 0 \tag{4.82}$$

$$K = (\mu(\nabla u + (\nabla u)^T) - \frac{2}{3}\mu(\nabla \cdot u)I \tag{4.83}$$

where u and ρ represent the velocity and density, respectively. The second term on the right side represent body force per unit volume. K is the coefficient of bulk viscosity. The equations of transport of species due to diffusion are described to find a mass fraction of species in the condenser. A mixture-averaged diffusion model which is a useful tool for variable partial pressures and temperature is used. The model equations are given below. In these equations, j_i and w_i are the mass flux and mass fraction term, respectively. D_i^T and ${D_i}^m$ represent thermal diffusion and mixture-averaged diffusion coefficient, respectively. Besides, M_i and x are the molecular weight and mole fraction, respectively.

$$\nabla \cdot j_i + \rho(u \cdot \nabla)w_i = R_i \tag{4.84}$$

$$j_i = -\left(\rho \cdot {D_i}^m \cdot \nabla w_i + \rho \cdot w_i \cdot {D_i}^m \frac{\nabla M_n}{M_n} - j_{c,i} + D_i^T \frac{\nabla T}{T}\right) \tag{4.85}$$

$$D_i^m = \frac{1-w_i}{\sum_{k \neq i} \frac{x_k}{D_{ik}}} \tag{4.86}$$

$$M_n = \left(\sum \frac{w_i}{M_i}\right)^{-1} \tag{4.87}$$

$$j_{c,i} = \rho w_i \sum \frac{M_i}{M_n} {D_k}^m \cdot \nabla x_k \tag{4.88}$$

The equations as shown below give the heat transfer between fluids in the condenser. The first term on the left-hand side of the first equation represents the total energy per unit volume, while the second term represents the rate of heat lost by conduction which is given in the following equation. Also, Q is the heat source. Q_p and Q_{vd} are other heat source terms due to pressure changes and viscous dissipation, respectively.

$$\rho c_p u \cdot \nabla T + \nabla \cdot q = Q + Q_p + Q_{vd} \tag{4.89}$$

$$q = -k \cdot \nabla T \tag{4.90}$$

The total vapor mass flux transported to liquid at the condensate flux is defined in Eq. (4.91) according to mass transfer laws (Baehr and Stephan, 2011). Here, h_m is the mass transfer coefficient and it can be found from the analogy between Nusselt and Sherwood (Eq. (4.92)). In Eq. (4.92), D represents the diffusivity constant while D_h represents the hydraulic diameter which is found in Eq. (4.93).

$${\dot{m}_{cond}}'' = \rho_{gas} \cdot h_m \cdot \ln\left(\frac{P - P_{sat}}{P - P_v}\right) \tag{4.91}$$

$$Sh = \frac{h_m \cdot D_h}{D} \tag{4.92}$$

$$D_h = \frac{4 \cdot A_c}{U} \tag{4.93}$$

where A_c is the area section of the duct while U is the wetted perimeter of the duct. After the final mass diffusivity condensate flux is calculated, the condensate heat rate can be calculated using Eq. (4.94). Here, Δh represents enthalpy of vaporizations.

$$\dot{q}_{cond} = {\dot{m}_{cond}}'' \cdot \Delta h \tag{4.94}$$

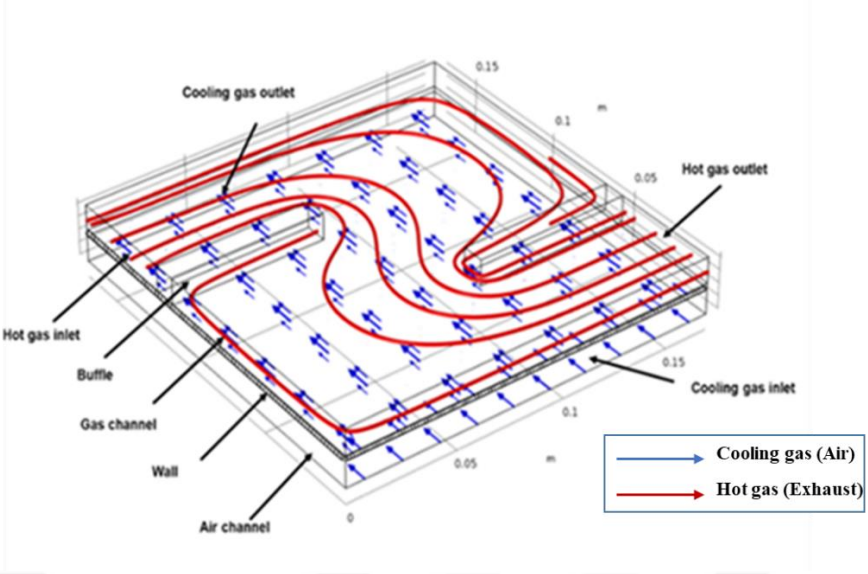

Figure 4.2 Air cooled condenser working principle

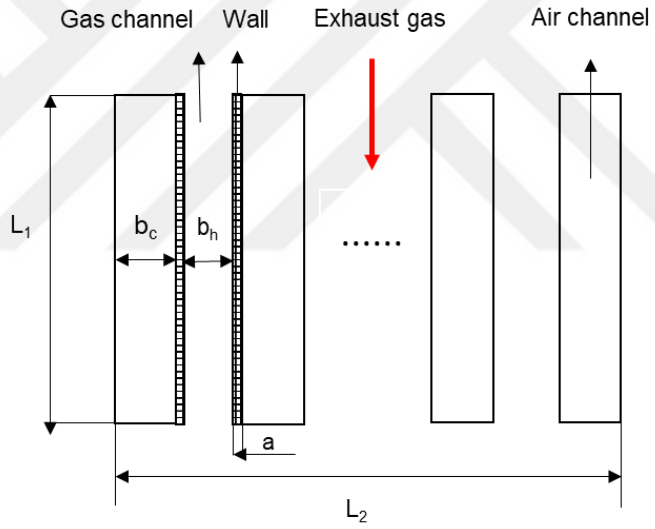

Figure 4.3 Geometry of condenser found in DMFC system

Table 4.6 Available condenser geometry parameters

Condenser parameters	Value	Condenser parameters	Value
Cooling gas inlet velocity	0.081 m/s	L_1 (Height of the condenser)	170 mm
Hot gas inlet velocity	0.05376 m/s	L_3 (Width of the condenser)	170 mm
Cooling gas (air) inlet temperature	25 °C	L_2 (Length of the condenser)	170 mm
The hot gas inlet temperature	70 °C	b_c (Length of the air channel)	10 mm
w_i (The inlet mass fraction of hot gas)	0.22	b_h (Length of the gas channel)	10 mm

Table 4.7 Calculation algorithm of two-phase condenser model

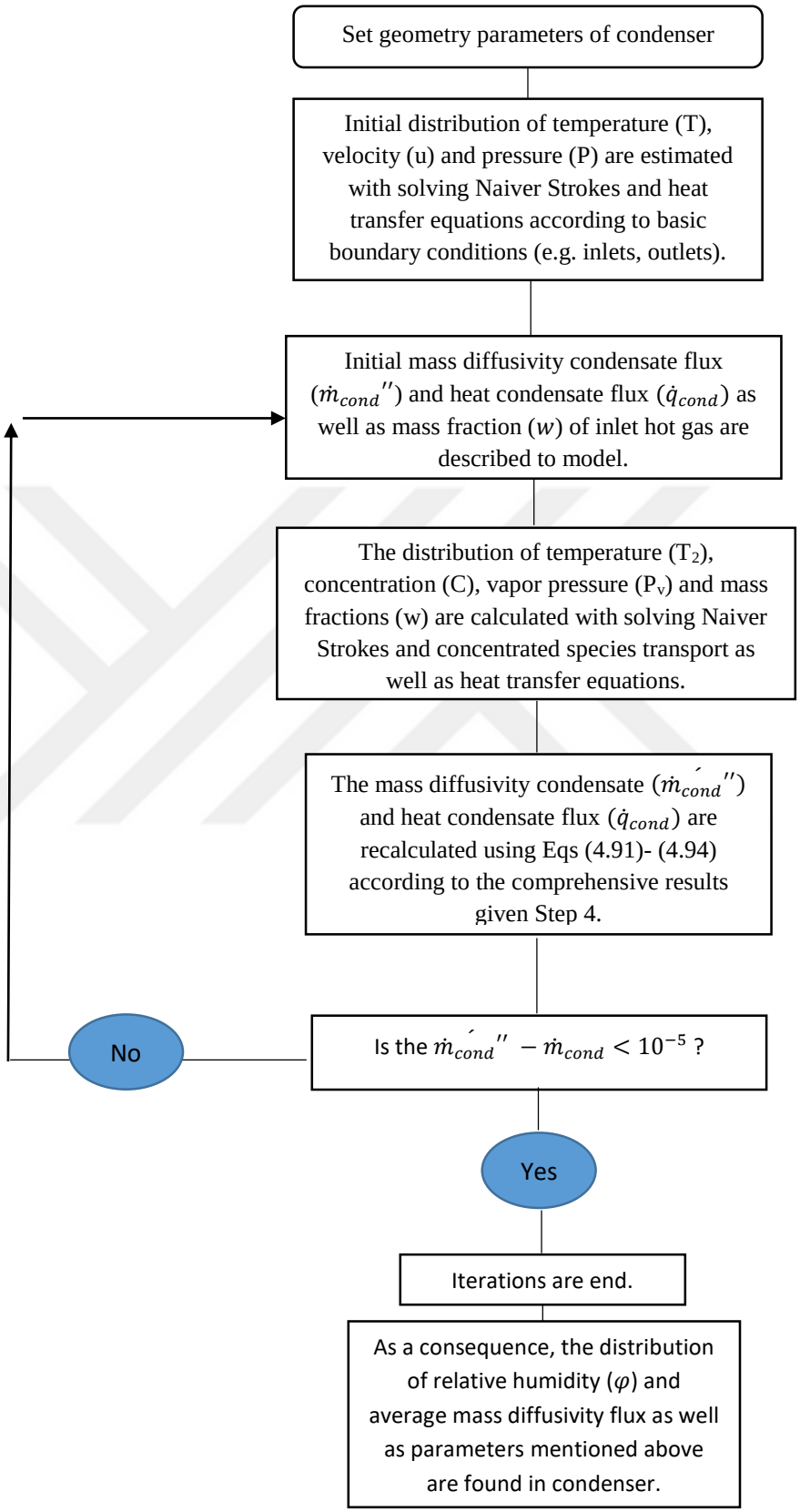

CHAPTER FIVE
RESULTS AND DISCUSSION

5.1 Introduction

A semi-empirical thermodynamic model of a DMFC system was developed. The empirical data are found. The set of equations given in Chapter 4 are then solved using the Engineering Equation Solver (EES) software to assess the system performance. In this chapter, the results and discussions of system analysis are given in different subsections. After the validation of results of system level model is presented, the mass fluxes of species for each state in DMFC system are given according to various concentrations. Secondly, power consumptions of auxiliary equipment, condenser outlet temperature and system electrical efficiency which are considered as performance assessment of energy analysis are presented for various air flow rate, methanol concentration and current density conditions. Finally, exergy analysis is studied. For this purpose, exergy flows for each state, exergy destructions for all components and exergetic efficiency of DMFC in cell and system level are studied at the same operating conditions given above. It should be noted that the results are given per total active area of the fuel cell (i.e., the active area of a single cell times the number of cells). In addition, the water autonomy provided by condenser is investigated. For this purpose, the two-phase model for available condenser is developed with following the calculation steps given Table 4.7. After validated this condenser model with literature, the mass condensate diffusivity flux is calculated for this condenser. Then, it is comprised with mass condensate diffusivity flux calculated with an approximate approach.

5.2 Validation

The system-level model developed is considered to be valid if the results obtained from the models of the main sub-components do compare reasonably well with those obtained experimentally or from literature. Since the polarization, methanol crossover, and water crossover curves of the DMFC are obtained experimentally, and they are

only used to find the mass flow rates at the inlet and exit of the anode and cathode sides, and the power density of DMFC, there is no need to validate the DMFC model. To validate the condenser model, which is based on the assumption that the relative humidity is 1 at the condenser inlet and outlet, the outlet temperature of the condenser was compared with the literature data. For this purpose, the computer code developed in the EES environment for the mathematical model was modified using the parameters (environmental temperature and humidity, and air stoichiometric ratio) given in the study of Zenith et al., 2010. When the condenser outlet temperatures were compared, the deviation between the current study and the study of Zeneith et al., 2010 was found be 3 %. In addition, the values found for the electrical efficiency of the system in the parametric studies were seen to be within the range given in the literature (Andrian and Meusinger, 2000; Nölke, 2007).

5.3 Energy Analysis of DMFC System

5.3.1 Mass Fluxes

The mass fluxes of fluids in the system were calculated for different values of methanol concentration. In the calculations, the current density and volume flow rate of air are taken as constant (0.20 $A \cdot cm^{-2}$ and 30 $mL \cdot cm^{-2} \cdot min^{-1}$, respectively) as shown in Table 5.1. This table shows that with an increase in the methanol concentration at the anode inlet (State 2), the methanol flow rate leaving the methanol tank and entering the anode side of the DMFC stack both increase considerably, as expected, according to the mass balance around the mixing chamber for the methanol (Eq. (4.7)). The main reason for this increase is that a higher methanol concentration causes an increase in the methanol crossover current density, as shown in Figure 3.3 For these reasons, the amount of water at the inlet of the anode decreases when the other operating parameters are taken as constant.

Recycling water, State 7, is vital for water autonomy in the system. If the mass balance is applied to the mixing chamber for water (Eq. (4.10)), it can be seen that the amount of water to be recycled depends on the water crossover and water consumption

rates. Here, the consumed water flow rate per active area in the anode is only a function of the current density. However, the water crossover rate changes with changing methanol concentration, current density, and air flow rate (Figure (3.4)). The mass flux of recycling water increases with an increase in the methanol concentration and required current density, but decreases with a decreased air flow rate, as the water crossover rate increases at a higher methanol concentration and current density and lower air flow rate conditions, as discussed in Chapter 3. Apparently, one of the key parameters is current density for water autonomy, as it affects both water crossover and water consumption at the anode. For example, if the current density increases from 0.10 to 0.15 $A \cdot cm^{-2}$, the mass flux of recycling water rate increases by 8%. However, the mass flux of the recycling water rate increases by 3.13% when the methanol concentration increases from 0.5 M to 1 M. Liquid water leaves the cathode outlet (State 6), in addition to H_2O_v and dry gas. In this study, it is found that when the methanol concentration increases, the mass flux of liquid water rate in the condenser outlet increases. The reason for the increment of the mass flux of the liquid water (recycling water) is that water production that occurs due to methanol crossover of the current density and water crossover inside the cell increases with increasing concentration when other operating parameters are taken as constant.

Table 5.1 Calculated mass flux for each state [$kg \cdot h^{-1} \cdot cm^{-2}$] for different methanol concentrations at a current density of 0.20 $A \cdot cm^{-2}$ and an air flow rate of 30 $mL \cdot cm^{-2} \cdot min^{-1}$

State	Substances	For 0.5 M	For 0.75 M	For 1 M	For 1.25 M
1	$CH_3OH_{(l)}$	0.00004228	0.00004670	0.00005328	0.00005904
2 and 3	$CH_3OH_{(l)}$	0.00022260	0.00033520	0.00044880	0.00056330
	$H_2O_{(l)}$	0.01324000	0.01312000	0.01301000	0.01306000
4	$CH_3OH_{(l)}$	0.00020980	0.00031990	0.00043060	0.00054220
	$H_2O_{(l)}$	0.01268000	0.01256000	0.01243000	0.01231000
	$CO_{2(g)}$	0.00005474	0.00005474	0.00005474	0.00005474
5	Air	0.00193200	0.00193200	0.00193200	0.00193200
	$O_{2(g)}$	0.00037140	0.00041320	0.00041320	0.00041320
	$N_{2(g)}$	0.00152300	0.00152300	0.00152300	0.00152300
	$H_2O_{(v)}$	0.00003828	0.00003828	0.00003828	0.00003828
6	$O_{2(g)}$	0.00030810	0.00030150	0.00029160	0.00028300
	$N_{2(g)}$	0.00152300	0.00152300	0.00152300	0.00152300
	$H_2O_{(v)}$	0.00052350	0.00052290	0.00052210	0.00052130
	$H_2O_{(l)}$	0.00009957	0.00011010	0.00013710	0.00015330
	$CO_{2(g)}$	0.00000330	0.00000940	0.00001845	0.00002635
	Total gas	0.00235800	0.00235700	0.00235500	0.00235300

Table 5.1 continues

7 and 9	$H_2O_{(l)}$	0.00055830	0.00056070	0.00057580	0.00058160
8	$O_{2(g)}$	0.00030810	0.00030150	0.00029160	0.00028300
	$N_{2(g)}$	0.00152300	0.00152300	0.00152300	0.00152300
	$H_2O_{(v)}$	0.00006478	0.00007223	0.00008334	0.00009304
	$CO_{2(g)}$	0.00000330	0.00000940	0.00001845	0.00002635
	Total gas	0.00180900	0.00190600	0.00191600	0.00192500
10	$CO_{2(g)}$	0.00005474	0.00005474	0.00005474	0.00005474

According to the mass analysis, the CO_2 in the anode outlet is primarily a function of the current density and is not influenced by a change in the methanol concentration and air flow rate. However, CO_2 in the cathode outlet is mostly a function of methanol concentration, which affects methanol crossover current density. Hence, as the methanol crossover current density increases with an increase in the methanol concentration, the mass flux of CO_2 increases at constant values of air flow rate and current density. However, an increase in the methanol concentration reduces the flow rate of O_2 leaving the cathode as it leads to an increase the consumption of O_2. The changes in the mass flux of H_2O_v is almost negligible because it mainly changes with temperature and air flow rate, as expected. As a result, the mass flux of total gas in the cathode outlet is almost equal to the sum of the amount of O_2, CO_2, H_2O_v, and N_2. When the methanol concentration increases at a constant air flow rate, the amount of change in the O_2 and CO_2 are equal to each other and thus, the mass flux of total gas in the cathode outlet, state 6, remains almost constant while other operating parameters are taken as constant. On the other hand, the air flow rate is the most influential parameter affecting the mass flux of total gas in the cathode outlet because when it increases, the mass flux of total gas in the cathode outlet increases significantly due to increasing H_2O_v, O_2 and N_2. When the air flow rate increases from 20 to 30 $mL \cdot cm^{-2} \cdot min^{-1}$, an increase of 49.65% in the amount of total gas in the cathode outlet was found.

The amount of dry gas, which is composed of O_2, N_2, and CO_2, does not change through the condenser; and they are released from the condenser outlet into the atmosphere. However, H_2O_v in the condenser outlet (Eq. (4.21)) is mainly related to the methanol crossover current density, the amount of H_2O_v in the cathode inlet and

the required current density. The amount of H_2O_v mass flux at the condenser outlet is an important parameter to determine the condenser outlet temperature, which is discussed in Section 5.3. As the methanol crossover current density increases with increasing methanol concentration, the mass flux of H_2O_v increases. Since the air flow rate is an operating parameter that has positive effects on both the methanol crossover current density and H_2O_v in the cathode inlet, the H_2O_v mass flux at the condenser outlet increases significantly. For example, when the air flow rate increases from 20 to 30 $ml \cdot cm^{-2} \cdot min^{-1}$ at a current density and methanol concentration of 0.20 $A \cdot cm^{-2}$ and 1 M, respectively, the mass flux of H_2O_v in the condenser outlet increases by 19.79%.

5.3.2 Electrical Efficiency of the System

The model described in Section 4 can be used to calculate the electrical efficiency of the system, which is one of the most important performance assessment parameters. This efficiency was calculated for different values of current density (0.05-0.25 $A \cdot cm^{-2}$), methanol concentration (0.5-1.25 M) and air flow rate (20-30 $mL \cdot cm^{-2} \cdot min^{-1}$). The results of these calculations are presented in Figure 5.1. This figure shows that comparatively higher values of electrical efficiency are achieved for the medium current density values (0.15-0.20 $A \cdot cm^{-2}$) when the methanol concentration is taken as 0.5 and 0.75 M, and the air flow rate is taken as 20 $mL \cdot cm^{-2} \cdot min^{-1}$.

It was discussed in Chapter 3 that the most important operating parameters affecting the cell voltage and methanol crossover current density are the current density and methanol concentration. For the range of current density values studied, the power density of the DMFC, which depends on the operating cell voltage and current density, reaches relatively higher values at higher current density, except the 0.5 M methanol concentration case. As the concentration polarization is more effective when a lower methanol concentration is used, there is a sharp decrease in the cell voltage for the 0.5 M case (Ren et al., 2002). For this reason, when the current density is taken as 0.25 $A \cdot cm^{-2}$, a lower power density and thus lower electrical efficiency is obtained for this case. Similarly, at this current density, although the power density is calculated at its highest value, 0.088 $W \cdot cm^{-2}$ (at a methanol concentration of 1.25 M and an air flow

rate of 30 $mL \cdot cm^{-2} \cdot min^{-1}$), the electrical efficiency of the system cannot reach its highest value, as shown in Figure 5.1. The main reason for this trend is that the higher methanol concentration significantly increases the methanol crossover current density and therefore the system efficiency decreases. When the air flow rate decreases from 30 $mL \cdot cm^{-2} \cdot min^{-1}$ to 20 $mL \cdot cm^{-2} \cdot min^{-1}$, the increase of electrical efficiency of the system is found be 12.5 % at methanol concentration of 0.75 M and a current density of 0.2 $A \cdot cm^{-2}$. The reason for the increase in the electrical efficiency is that when the air flow rate decreases, methanol crossover current density (Figure (4.3)) and power consumption of the blower decrease (Eq. (4.26)). Eventually, when the methanol concentration, air flow rate and current density are taken as 0.75 M, 20 $mL \cdot cm^{-2} \cdot min^{-1}$ and 0.2 $A \cdot cm^{-2}$ (at 0.387 V), respectively, the highest electrical efficiency of the system is obtained at 23.6%.

As is conveyed in Eq. (4.26), the higher power output of the cell and lower power consumption of auxiliary equipment yield higher overall electrical efficiency. Hence, the change of these parameters with the input parameters should be assessed in order to understand the effects of these parameters on the electrical efficiency of the overall system. Figures 5.2-a and 5.2-b show the change of the total power density consumed by auxiliary units, the power density of the fuel cell and net power density of the system with respect to methanol concentration and air flow rate. Here, due to low-pressure change between the inlet and outlet of the blower and pumps in the system, the main factor affecting the power consumption of the auxiliary equipment becomes the mass flux of each species entering these components, as discussed in Chapter 5.3.1 It can be observed in Figure 5.2-b that when the air flow rate increases from 20 $mL \cdot cm^{-2} \cdot min^{-1}$ to 30 $mL \cdot cm^{-2} \cdot min^{-1}$, the total auxiliary power consumption increases from 0.0167 $W \cdot cm^{-2}$ to 0.025 $W \cdot cm^{-2}$ due to the fact that power consumption of the blower increases from 0.0166 $W \cdot cm^{-2}$ to 0.025 $W \cdot cm^{-2}$. On the other hand, because of the low flow rate of the anode (0.23 $mL \cdot cm^{-2} \cdot min^{-1}$), the fuel pump consumes very little power (1.92×10^{-5} $W \cdot cm^{-2}$). Similarly, recycling and methanol pumps also feature low power densities, which are calculated as 6.34×10^{-7} $W \cdot cm^{-2}$ and 4.15×10^{-7} $W \cdot cm^{-2}$, respectively, for an air flow rate, current density and methanol concentration of 30 $mL \cdot cm^{-2} \cdot min^{-1}$, 0.10 $A \cdot cm^{-2}$, and 0.5 M, respectively.

5.3.3 Condenser Outlet Temperature

Another major output parameter of the model is the condenser outlet temperature, which determines the condenser's heat duty. The change in this temperature, according to the air flow rate, methanol concentration and current density, is shown in Figure 5.3 To calculate the condenser outlet temperature, the mass flux of H_2O_v is first calculated using Eq. (5.1), which is found by rearranging the condenser mass balance (Eq. (4.21)) and Eqs. (4.12) and (4.20):

$$\dot{m}''_{8,H_2O_{(v)}} = \dot{m}''_{H_2O,gen_{ec}} + \dot{m}''_{H_2O,gen_{mc}} + \dot{m}''_{5,H_2O_{(v)}} - \dot{m}''_{H_2O,cons} \qquad (5.1)$$

Here, water produced ($\dot{m}''_{H_2O,gen_{ec}}$) and water consumed ($\dot{m}''_{H_2O,cons}$) due to ORR are mainly functions of current density; while the produced water ($\dot{m}''_{H_2O,gen_{mc}}$) due to MOR is mostly a function of methanol crossover current density. Saturation pressure of the condenser outlet ($P_8, sat, H_2O_{(v)}$) is then found by inserting Eq. (5.1) into Eq. (4.22). Finally, using Antoine's equation (Eq. (4.24)), the cathode outlet temperature is calculated.

The current density leads to an increase in the mass flux of H_2O_v at the condenser outlet because the water produced by the current density is more than the water consumed by it. However, as increasing current density decreases methanol crossover current density, the amount of O_2 remains almost constant at the cathode outlet for a given air flow rate. Similarly, as the methanol crossover current density decreases with an increase in the current density, the increase of the mass flux of CO_2 due to increase of methanol crossover current density is negligible. Therefore, the mass flux of dry gas at the cathode outlet remains almost constant with an increase current density while air flow rate and methanol concentration are constant. As the increased mass flux of vapor leads to a slight increase in the pressure of the condenser outlet, the condenser outlet temperature increases while other operating conditions are taken as constant. The condenser outlet temperature reaches higher values at higher methanol concentrations while other operating conditions are taken as constant. The increase of condenser outlet temperature is found be 14.47 %, when the methanol concentration

is increased from 0.75 M to 1.25 M while current density and air flow rate are taken as 0.05 $A \cdot cm^{-2}$ and 20 $ml \cdot cm^{-2} \cdot min^{-1}$, respectively. It can be explained that higher methanol concentration causes an increase in the methanol crossover current density, which leads to an increase in the mass flux of H_2O_v, as well as dry gas (due to increased CO_2). On the other hand, the air flow rate plays a key role in determining the condenser's outlet temperature. The cathode outlet temperature increases with an increasing air flow rate owing to the fact that this flow rate leads to an increase in the H_2O_v flux at the cathode outlet. For example, to increase the cathode outlet temperature by 5 °C, the air flow rate is increased from 20 $mL \cdot cm^{-2} \cdot min^{-1}$ to 30 $ml \cdot cm^{-2} \cdot min^{-1}$ because when the air flow rate is increased, as the total gas flux at the cathode outlet increases rapidly, the saturated pressure decreases. The decreased saturated pressure of the condenser outlet, in turn, leads to an increase in the temperature gradient between the condenser inlet and outlet. The highest condenser outlet temperature (47.2 °C) is obtained at an air flow rate of 20 $mL \cdot cm^{-2} \cdot min^{-1}$ when the current density and methanol concentration are taken as 0.25 $A \cdot cm^{-2}$ and 1.25 M, respectively.

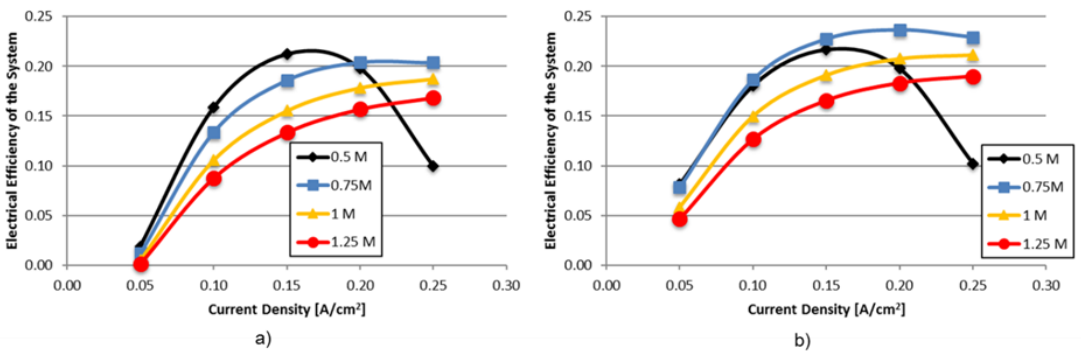

Figure 5.1 Effect of methanol concentrations (0.5, 0.75, 1 and 1.25 M) and air flow rates of: a) 30 $mL \cdot cm^{-2} \cdot min^{-1}$; b) 20 $mL \cdot cm^{-2} \cdot min^{-1}$ on the electrical efficiency of the system

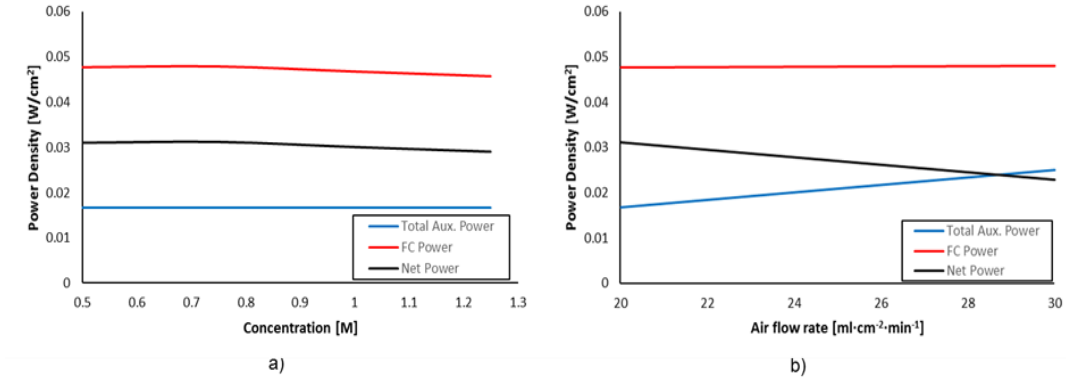

Figure 5.2 Change of total power density consumed by the auxiliary components, the power density generated by the fuel cell and the net power output density for different values of: a) methanol concentration at the air flow rate of 20 mL·cm^{-2}·min^{-1}, current density of 0.10 A·cm^{-2}; and b) air flow rate at the methanol concentration of 0.5 M, current density of 0.10 A·cm^{-2}

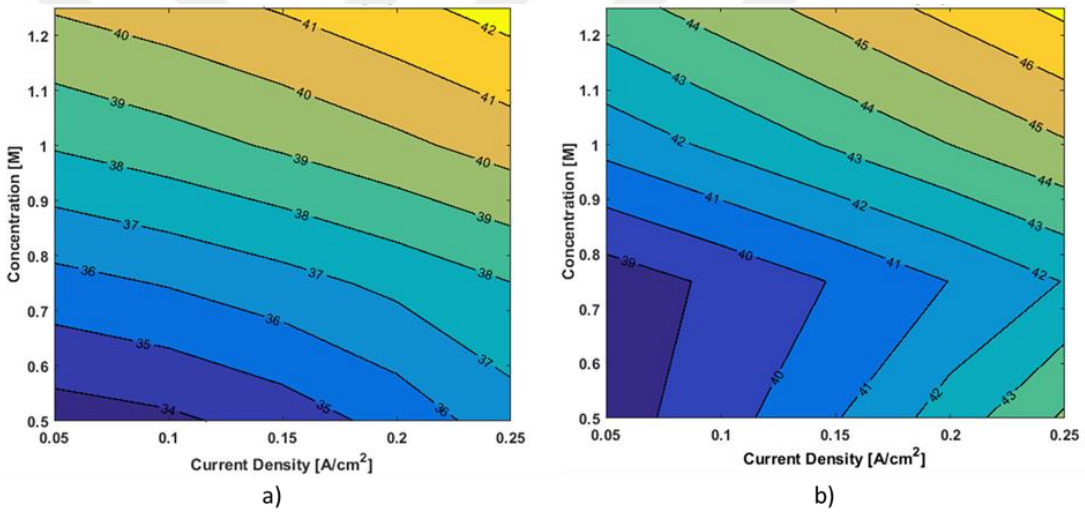

Figure 5.3 The condenser outlet temperatures at an air flow rate of: a) 30 mL·cm^{-2}·min^{-1}; and b) 20 mL·cm^{-2}·min^{-1}

5.4 Exergy Analysis of DMFC System

In this thesis, after the energy analysis on DMFC system with using semi-empirical model, the exergy analysis is conducted. In this section, the effect of methanol concentration, current density and air flow rate on exergetic efficiency of DMFC in cell and system level is investigated. In addition, exergy destructions of main components (condenser, DMFC and auxiliary equipment) are examined parametrically

according to these conditions given above. For this purpose, exergy flows are calculated for each state as shown in Table 5.2.

5.4.1 Exergy Flows

It is found that the temperature and pressure differences between inlet and outlet of pumps are negligible due to the low power consumption of pumps as shown Fig. (5.2). Therefore, exergy flows at the inlet and outlet of pumps are considered as the same. In addition, the total exergy flow rate of State 10 that includes CO_2 species is calculated as 0 due to the fact that the physical conditions at that state correspond to dead state (physical exergy), and CO_2 component is negligible at dead state (chemical exergy). The highest exergy flow rate is calculated at state 1. It can be explained that the standard molar chemical exergy of methanol as shown Table 3.2 is much higher due to higher Gibbs function of the formation. It should be pointed out that the change of exergy flow rate depends on physical conditions (temperature and pressure) and chemical compositions.

Table 5.2 Total exergy flow rates for each state at methanol concentration, air flow rate and current density of 0.75 M, 20 $mL \cdot cm^{-2} \cdot min^{-1}$ and 0.10 $A \cdot cm^{-2}$, respectively

State No.	Total $\overline{ex}$ flow [kJ/kmol]
1	718000
2 and 3	701609
4	701729
5	205
6	9963
7 and 9	68
8	1955
10	0
11	14910
12	6251

In addition, the total exergy flow of state 10 that includes CO_2 species is calculated as 0 due to the fact that the physical conditions at that state correspond to dead state (physical exergy), and CO_2 component is negligible at dead state (chemical exergy). The highest exergy flow is calculated at state 1. It is explained that the standard molar chemical exergy of methanol as shown Table 3.2 is very higher due to higher Gibbs function of the formation. It should be pointed out that the change of exergy flow depends on physical conditions (temperature and pressure) and chemical compositions.

5.4.2 Exergetic Efficiency

In Figures (5.4) and (5.5), the change of exergetic efficiency of DMFC in system level due to methanol concentration is shown for air flow rate of 20 and 30 $mL \cdot cm^{-2} \cdot min^{-1}$, respectively. Here, a decrease of exergetic efficiency is observed with an increase of methanol concentration. According to Eq. (4.4), it is explained that molar flux of methanol entering the system is increased by increasing methanol concentration as given in Table (5.1). In addition, net power output of DMFC is decreased slightly with an increase of methanol concentration. The exergetic efficiency of DMFC in cell level is investigated in Figures (5.6) and (5.7). The products and reactants exergy flow and mass fluxes are important parameters as well as fuel cell power to determine exergetic efficiency of DMFC as given Eq. (4.80). The investigation of fuel cell power and mass fluxes for different methanol concentrations are discussed in Section 5.3.

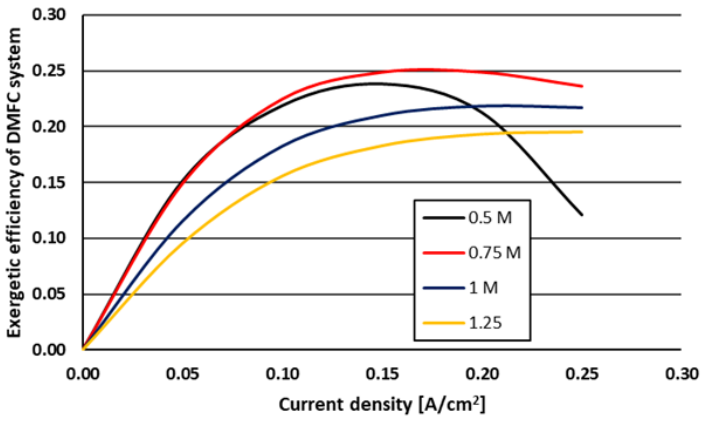

Figure 5.4 Effect of various methanol concentrations and current densities on exergetic efficiency of DMFC in system level at air flow rates of 20 $mL \cdot cm^{-2} \cdot min^{-1}$

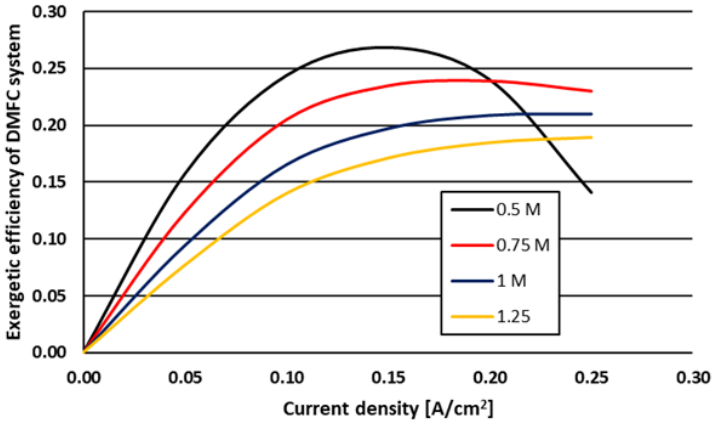

Figure 5.5 Effect of variable methanol concentrations and current densities on exergetic efficiency of DMFC in system level at air flow rates of 30 mL·cm^{-2}·min^{-1}

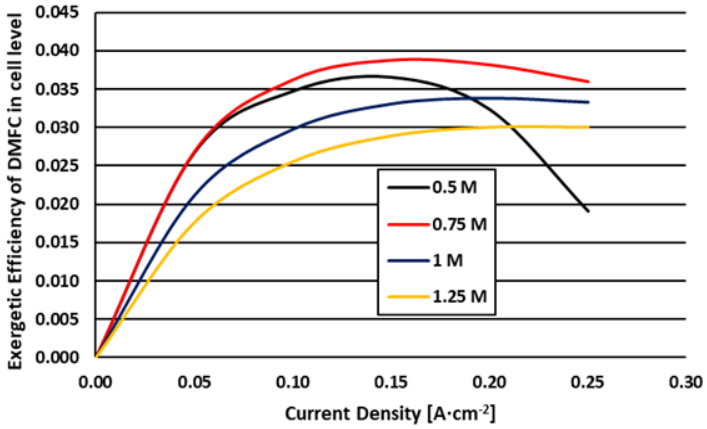

Figure 5.6 Effect of variable methanol concentrations and current densities on exergetic efficiency of DMFC in cell level at air flow rates of 20 mL·cm^{-2}·min^{-1}

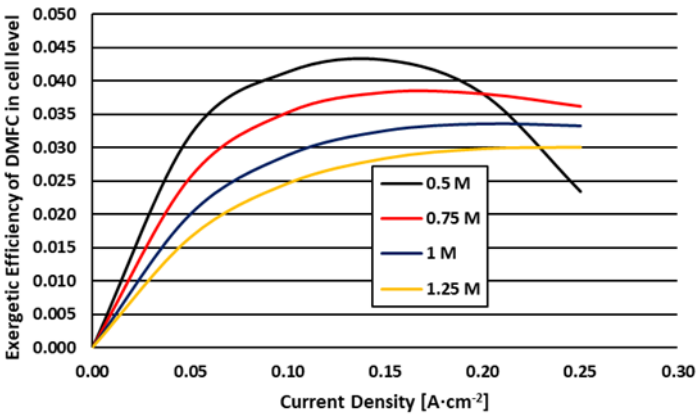

Figure 5.7 Effect of variable methanol concentrations and current densities on exergetic efficiency of DMFC in cell level at air flow rates of 30 mL·cm^{-2}·min^{-1}

Another important remark is that both system and cell exergetic efficiency are first increasing at lower current densities for each concentration value as shown Figures (5.4-5.7). After reaching peak point, it decreases with an increasing current density. Apparently, the low consumption of fuel entering to the system and cell leads to increase exergetic efficiency until reaching peak values. However, after the peak value, the reason of decreasing exergetic efficiency is due to an increase in fuel consumption. For example, the peak values are obtained as 60 % and 27 % at low current density regime when the air flow rate is 30 $ml \cdot cm^{-2} \cdot min^{-1}$ for DMFC in cell and system level, respectively. This finding shows good agreement with the trend of exergetic efficiency found by Hussain et al. (2005). The differences in peak values between cell and system level can be explained with the transportation of different molar exergy flow and mass fluxes of species to the system and cell.

The effect of air flow rate on the exergetic efficiency for DMFC in cell and system level is also investigated. It is shown that with the increase of air flow rate results in increase of exergetic efficiency of DMFC cell level, especially at lower methanol concentrations. An increment of exergetic efficiency of cell is found as 100 %, when the air flow rate increases from 20 $mL \cdot cm^{-2} \cdot min^{-1}$ to 30 $mL \cdot cm^{-2} \cdot min^{-1}$ at methanol concentration and current density of 0.5 M and 0.05 $A \cdot cm^{-2}$, respectively. However, the increment is calculated as 6.7 %, when the air flow rate increases from 20 $mL \cdot cm^{-2} \cdot min^{-1}$ to 30 $mL \cdot cm^{-2} \cdot min^{-1}$ at methanol concentration and current density of 1.25 M and 0.05 $A \cdot cm^{-2}$, respectively. The reason is obviously due to the lower fuel consumption at 0.5 M concentration. On the other hand, the effect of air flow rate on the system exergetic efficiency is limited by required methanol for the system and the power consumption of blower. Since the power consumption of blower increases with an increasing air flow rate, net power density decreases and thus exergetic efficiency decreases. The decrement of exergetic efficiency is calculated as 24 % when the air flow rate increases from 20 to 30 for 0.05 $A \cdot cm^{-2}$ current density at methanol concentration of 1.25 M.

5.4.3 Exergy Destruction Rates

In this section, the exergy destructions which are an important part of exergy analysis due to fact that it represents irreversibilities in system components are given for each component of DMFC system. The exergy destructions can be occurred due to friction, expansion, mixing, chemical reaction, and heat transfer. To find exergy destructions in system components, the equations given in Table 4.5 are applied to these components. The exergy destruction rates of condenser are given in Figures (5.8) and (5.9) for variable methanol concentrations at air flow rates of 30 $ml \cdot cm^{-2} \cdot min^{-1}$ and 20 $mL \cdot cm^{-2} \cdot min^{-1}$, respectively. When the methanol concentration increases from 0.5 M to 1.25 M, the exergy destruction rates decreases. For example, while the exergy destruction rates of condenser are found as 2.7 W at 0.5 M methanol concentration, it is calculated as 2.4 W at 1.25 M methanol concentration. Similarly, with an increase of air flow rate, the exergy destruction of condenser significantly decreases. When the air flow rate increases from 20 $mL \cdot cm^{-2} \cdot min^{-1}$ to 30 $mL \cdot cm^{-2} \cdot min^{-1}$, the exergy destruction rates of condenser increases almost of the 60 % at methanol concentration of 0.5 M while other parameters are taken as constant. This increment is also observed for other methanol concentrations value. The reason of this increment is because the mass fluxes entering the condenser increase significantly with an increase air flow rate. In addition, exergy flow leaving the condenser decreases due to decrement of condenser outlet temperature with increasing air flow rate. Another important parameter which effects on the exergetic destruction of condenser is the current density. The effect of current density on the exergetic destruction of condenser is given in Table 5.3 for 30 and 20 $mL \cdot cm^{-2} \cdot min^{-1}$ air flow rates while other parameters are constant. The table illustrates the exergy destruction rates decreases slightly with an increase of current density. This decrement is found as 3.2 % when the current density increases from the 0.05 to 0.25 $A \cdot cm^{-2}$ at air flow rate of 30 $mL \cdot cm^{-2} \cdot min^{-1}$. Similar results are also observed at 20 $mL \cdot cm^{-2} \cdot min^{-1}$. The lower decrement of the exergy destruction in condenser with a rise of current density is because of increment of the condenser outlet temperature when the current density increases. Hence, the temperature gradient between condenser inlet and outlet decreases. In this case, the irreversibilites due to temperature differences decrease.

The change of exergy destruction in DMFC is shown Figures (5.10) and (5.11) according to various air flow rate and methanol concentration. The increase of methanol concentration, unlike the condenser, leads to increase exergy destruction of DMFC. For example, the increment of exergy destruction rates of DMFC are calculated as 0.04 W and 0.14 W at methanol concentrations of 0.5 M and 1.25 M while other parameters are taken constant. Similar results are observed at study of Bahrami and Faghri (2011) who are conducted research on exergy analysis of DMFC in cell level. They explained that this increment of exergy destruction rates in DMFC is because of resistance of electric, the electrochemical reaction, multicomponent flows, phase change of condensable species as well as friction of ions.

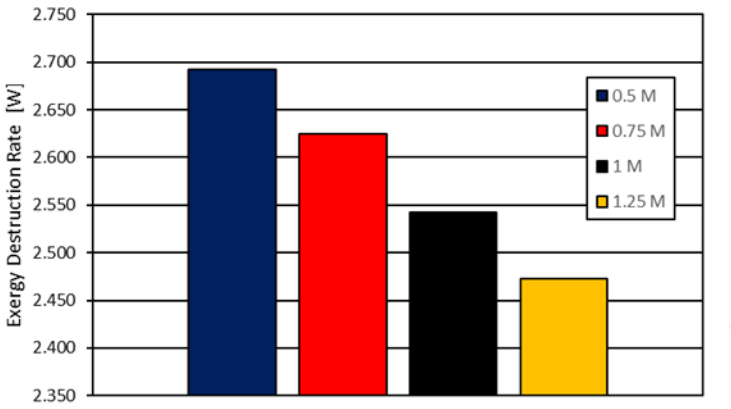

Figure 5.8 The change of exergy destruction rates of condenser due to methanol concentration at current density and air flow rate of 0.1 $A \cdot cm^{-2}$ and 30 $mL \cdot cm^{-2} \cdot min^{-1}$, respectively

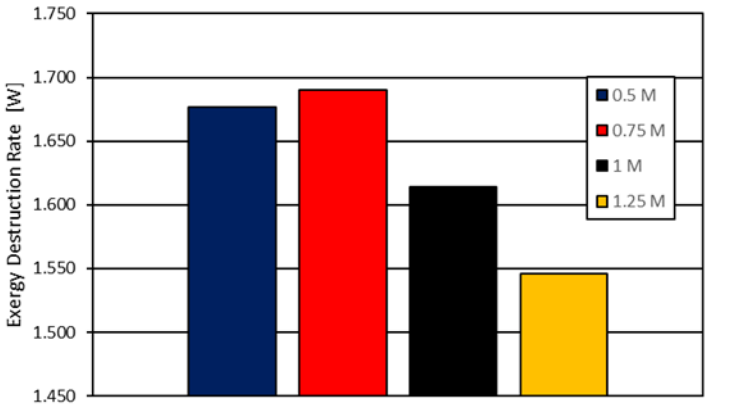

Figure 5.9 The change of exergy destruction rates of condenser due to methanol concentration at current density and air flow rate of 0.1 $A \cdot cm^{-2}$ and 20 $mL \cdot cm^{-2} \cdot min^{-1}$, respectively

Table 5.3 The change of current density on the exergy destruction rates of condenser for 0.75 M methanol concentration at air flow rate of 30 and 20 mL·cm^{-2}·min^{-1}

Air flow rate (mL·cm^{-2}·min^{-1})	Current density, i (A·cm^{-2})	Exergy destruction rate of condenser, $\dot{E}x_{D_{cond}}$ (W)
30	0.05	2.65
	0.10	2.62
	0.15	2.60
	0.20	2.59
	0.25	2.57
20	0.05	1.71
	0.10	1.69
	0.15	1.67
	0.20	1.65
	0.25	1.63

The effect of current density on the exergy destruction of DMFC is also examined in Table 5.4. The results show that the increment of current density leads to increase of exergy destruction rates of DMFC. This increment is calculated as 30 %, when the current density increases from 0.15 to 0.20 A·cm^{-2} for constant other parameters. However, this increment is found as 50 % when the current density increases from 0.05 to 0.10 A·cm^{-2}. Although the increment of current density is the same in above, Although the increment of current density is the same in above, the increment of exergy destruction rates of DMFC is more at the change of low current density regime. The reason is that power density of DMFC has increasing trend at the lower current density regime. Hence, the irreversibilities due to work increases significantly at lower current density regime when the compared with higher current density regime. In this study, the results of exergy destruction rate of DMFC with change of current density show the good agreement with the study of Ay, Midilli, & Dincer (2006).

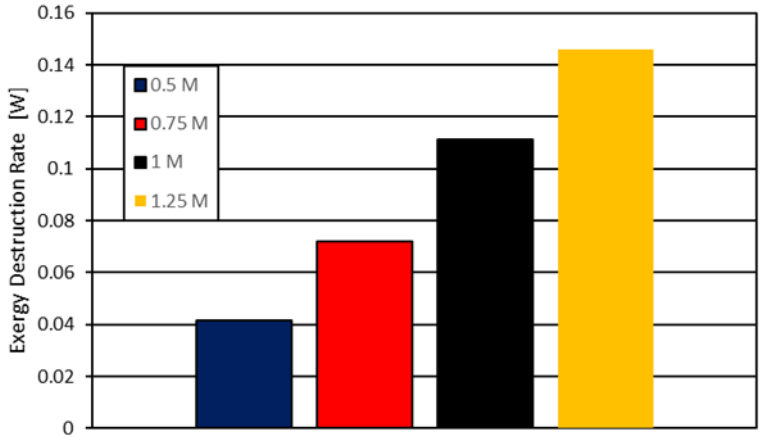

Figure 5.10 The change of exergy destruction rates of DMFC due to methanol concentration at current density and air flow rate of 0.1 A·cm^{-2} and 30 mL·cm^{-2}·min^{-1}, respectively

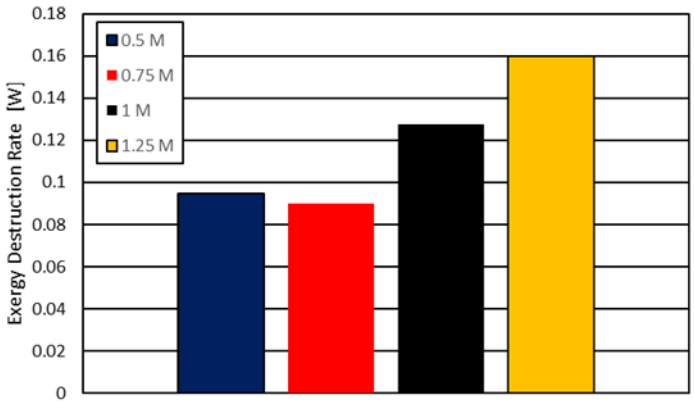

Figure 5.11 The change of exergy destruction rates of DMFC due to methanol concentration at current density and air flow rate of 0.1 A·cm^{-2} and 20 mL·cm^{-2}·min^{-1}, respectively

Table 5.4 The change of current density on the exergy destruction rates of DMFC for 0.75 M methanol concentration at air flow rate of 30 and 20 mL·cm^{-2}·min^{-1}

Air flow rate (mL·cm^{-2}·min^{-1})	Current density, i (A·cm^{-2})	Exergy destruction rate of DMFC, $\dot{E}x_{D_{DMFC}}$ (W)
30	0.05	0.04
	0.10	0.07
	0.15	0.10
	0.20	0.13
	0.25	0.17

Table 5.4 continues

20	0.05	0.06
	0.10	0.09
	0.15	0.12
	0.20	0.15
	0.25	0.20

Similarly, the effect of methanol concentration and air flow rate on the total exergy destructions of other system equipment (blower, methanol tank, mixing chamber and pumps) are examined parametrically for constant current density as shown Figures (5.12) and (5.13). The highest exergy destruction rates are obtained in methanol tank and blower. The important reason that lead to the unsatisfactory performance of exergy destruction rate of methanol tank, is that pure methanol which transports higher chemical exergy (718000 $kJ \cdot kmol^{-1}$) than diluted solutions leaves the methanol tank. The reason of high exergy destruction rates in blower is that high mass fluxes entering the blower. As a consequence, the parameters (e.g. increasing methanol concentration) that increase exergy flow of methanol lead to increase of exergy destruction of other system equipment. Besides, the parameters that increase the mass fluxes (e.g. increasing air flow rate) results with increase of the exergy destruction rates of other system equipment. For example, when methanol concentration increases from 0.5 M to 1.25 M, the exergy destruction rates increase the 31.1 %. In addition, the increment of exergy destruction rates of these components are found as 6.7%, when the air flow rate increases from 20 $mL \cdot cm^{-2} \cdot min^{-1}$ to 30 $mL \cdot cm^{-2} \cdot min^{-1}$.

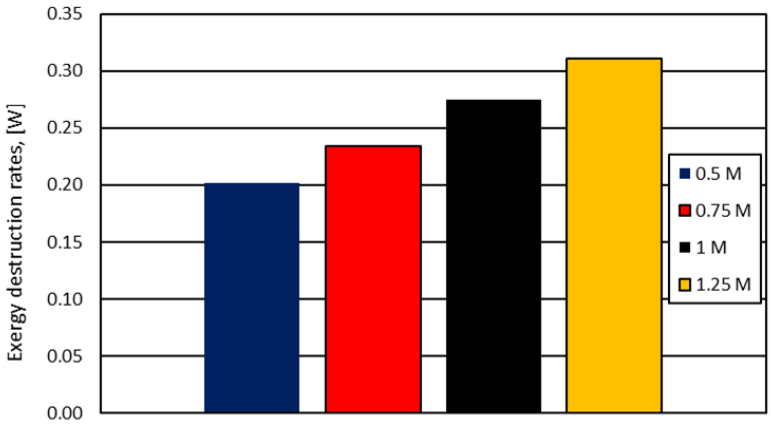

Figure 5.12 The change of exergy destruction rates of auxiliary equipment due to methanol concentration at current density and air flow rate of 0.1 $A \cdot cm^{-2}$ and 30 $mL \cdot cm^{-2} \cdot min^{-1}$, respectively

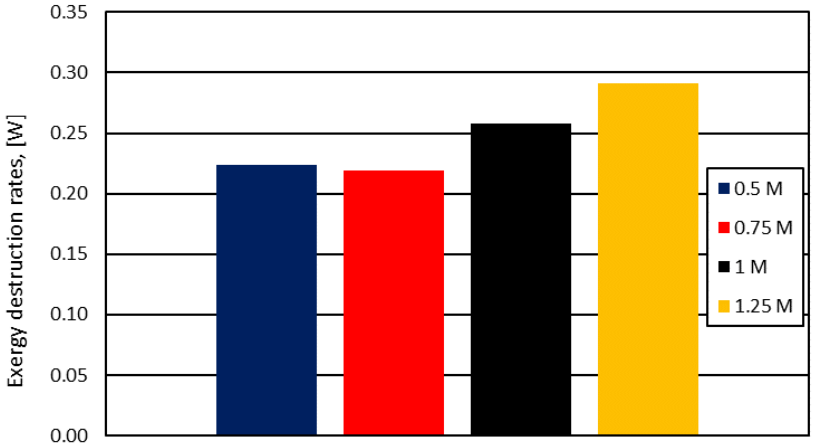

Figure 5.13 The change of exergy destruction rates of auxiliary equipment due to methanol concentration at current density and air flow rate of 0.1 $A \cdot cm^{-2}$ and 20 $mL \cdot cm^{-2} \cdot min^{-1}$, respectively

5.5 Water Autonomy for DMFC System

A 3-D CFD model in COMSOL 5.4 is first developed for an available condenser in DMFC systems to investigate water autonomy for this condenser. Then, the mass diffusivity flux according to available condenser ability is calculated as well as condensate heat flux using this model. In addition, the distribution of relative humidity (Figure 5.14-a), vapor pressure (Figure 5.14-b), mole fraction (Figure 5.15-a) and temperature (Figure 5.15-b) which effect the water autonomy are investigated in detail through the condensate side of condenser.

The hot gas enters the condenser as saturated (100%) and remains saturated during the cooling process as shown in Figure 5.14-a as expected. However, it is obtained that there is a region that the condensation cannot occur under the saturation point for this condenser. Since the vapor content in hot gas decreases due to condensation, the vapor pressure decreases as shown in Figure 5.14-b. Similarly, Figure 5.15-a shows that the mole fraction decreases along with the condenser. It should be noted that the line of Figure 5.15-a is interrupted due to baffles. When the hot gas reaches the outlet, the relative humidity, vapor pressure and mole fraction are found as 1, 0.05 bar and 0.05, respectively.

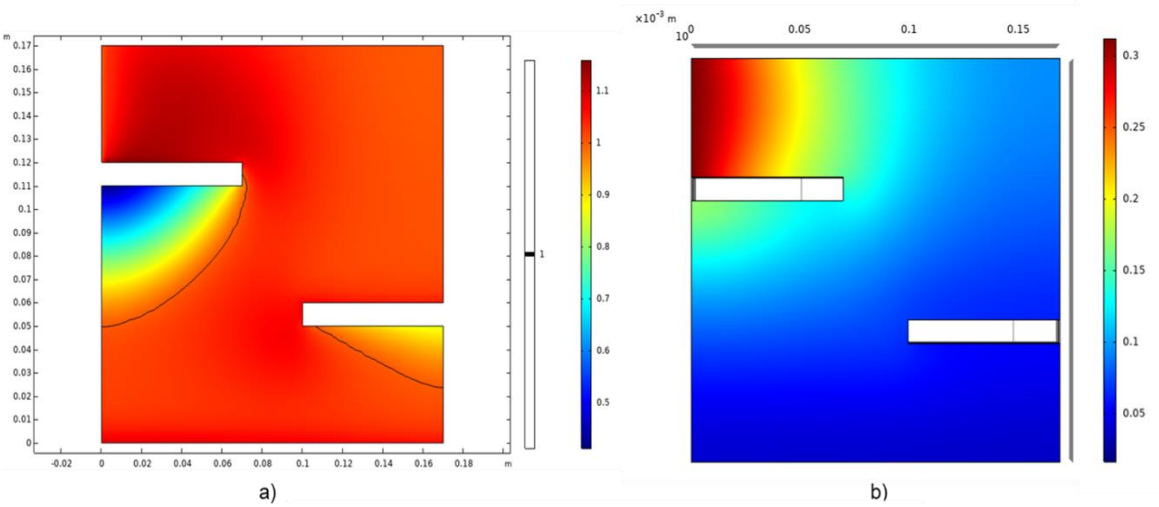

Figure 5.14 The simulation results of a) relative humidity b) vapor pressure

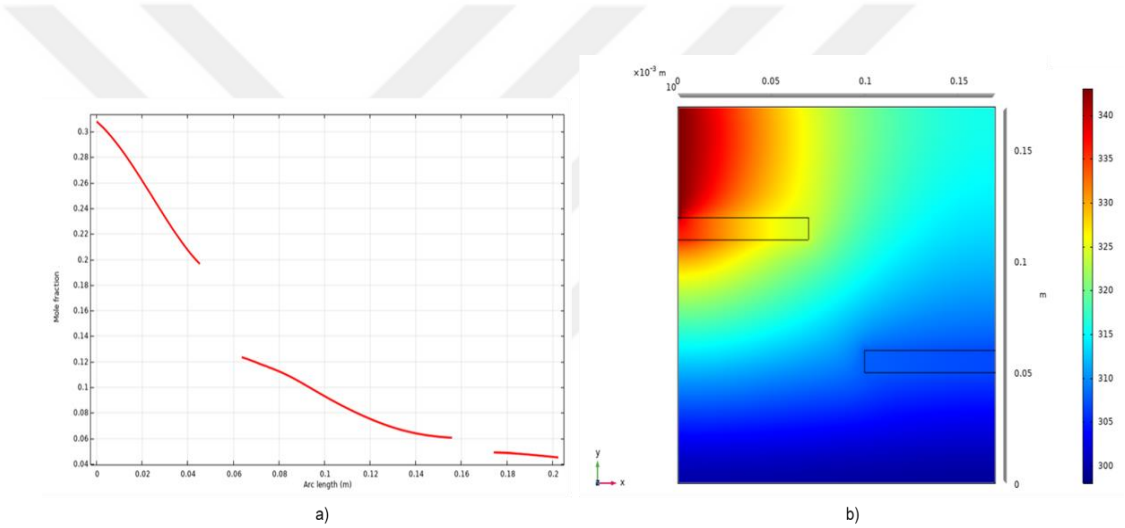

Figure 5.15 The simulation results of a) mole fraction b) temperature

Figure 5.15-b shows that temperature decreases along the condenser. This decrement of temperature is due to condensation and convection heat transfer. The convection heat flux which cools down the non-condensable gas is equals to the total heat transfer obtained from applying the energy balance to control volume of condensate side of condenser minus condensation heat flux calculated from Eqs. (4.91) -(4.94). The effect of heat transfers due to convection on cooling down of temperature of exhaust gas is very low. The temperature profile for heat transfer governed by convection is shown in Figure 5.16 during z direction. This temperature profile shows the good agreement with the literature (Baehr and Stephan 2011). The temperature decrement is found as 0.6 K due to convection heat transfer.

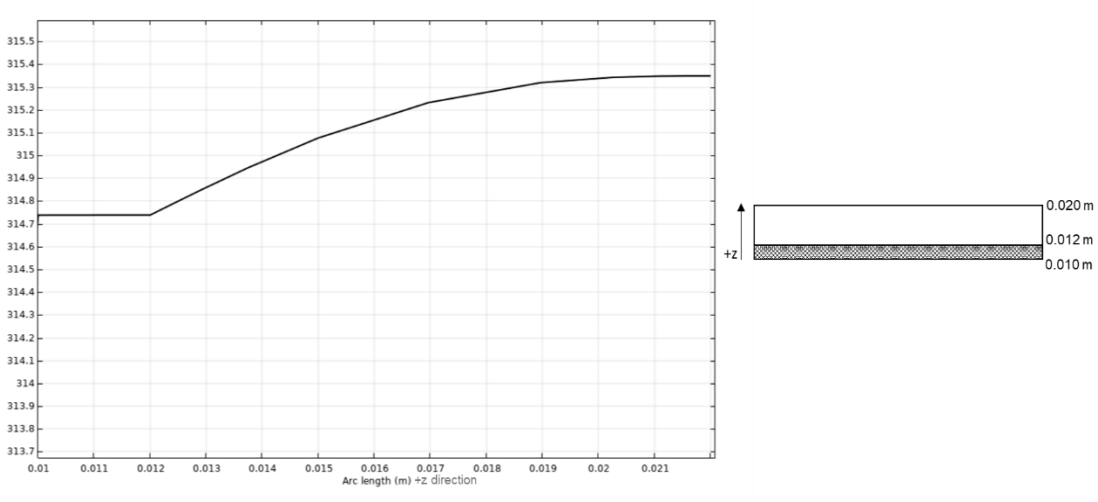

Figure 5.16 The effect of non-condensable gas on the temperature profiles

After the two-phase modeling of condenser, the water autonomy is investigated. Considering this model, it is known that how much water vapor condensate for an available condenser. Similarly, the amount of water of system required from the condenser is calculated an approximate approach using Eq. (5.2). For example, while the mass condensate diffusivity flux according to system requirement is found as 0.00004491 $kg \cdot m^{-2}$, the available condenser give the mass condensate diffusivity flux as 0.00001670 $kg \cdot m^{-2}$ when methanol concentration, current density and air flow rate are 0.5 M, 0.05 $A \cdot cm^{-2}$ and 30 $mL \cdot cm^{-2} \cdot min^{-1}$, respectively. It is seen that the condensate ability of condenser is lower than the system requirements.

$$\dot{m}''_{cond_{system}} = \dot{m}''_{H_2O,7} - \dot{m}''_{H_2O,6} \tag{5.2}$$

The difference of mass condensate diffusivity flux between condenser ability and system requirement is shown Figure (5.17) according to various air flow rate and current density. It is represented as $\dot{m}''_{cond_{differ}}$ which can be found using Eq. (5.3). For this condenser, the mass condensate diffusivity flux of system requirement is higher than condenser ability for variable operating conditions. Therefore, the water autonomy cannot be provided. However, the mass condensate diffusivity flux differences between system requirements and condenser ability decreases when the air flow rate decreases. For example, this differences are found as 0.00003 $kg \cdot s^{-1} \cdot m^2$ and

0.00005 kg·s^{-1}·m^{2} at air flow rate of 20 mL·cm^{-2}·min^{-1} and 30 mL·cm^{-2}·min^{-1}, respectively. The reason of decrease the differences mass condensate diffusivity flux with a decreasing air flow rate is that when the air flow rate decreases, the amount of recycling water ($\dot{m}''_{H_2O,7}$) decreases significantly as discussed Section 5.3.1. In addition, as the velocity of hot gas entering the condenser decreases with a decreasing air flow rate, the $\dot{m}_{cond}''$ decreases. Both decreasing recycling water and velocity of hot gas provide to decrease the differences of mass condensate diffusivity flux between system requirements and condenser ability. Similarly, when the current density increases, this gap decreases due to the reasons discussed above.

$$\dot{m}''_{cond_{differ}} = \dot{m}''_{cond_{system}} - \dot{m}_{cond}'' \quad (5.3)$$

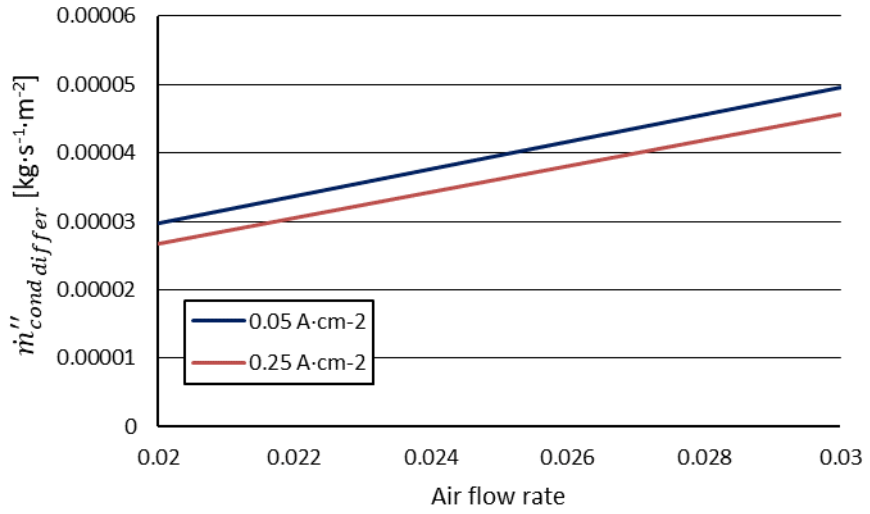

Figure 5.17 Effect of air flow rate on the mass condensate flux differences between system requirement and condenser ability for 0.05 A·cm^{-2} and 0.25 A·cm^{-2} current density

CHAPTER SIX
CONCLUSION

A semi-empirical model for DMFC system was developed to understand better DMFC system performance. To obtain empirical data, experiments which include the polarization curve as well as the methanol and water crossover curves according to air flow rate, current density and methanol concentration were done at single cell experimental test setups which were custom-made at the Forschungszentrum Jülich. Besides, the short stack experiments according to air flow rate, methanol permeation and current density were performed at short stack experimental test setups at the same institution. Consequently, the comparison of the performance results between single cell and short stack were performed to understand abilities of each of the two approach in terms of DMFC characterization. The important findings based on single cell performance are listed as follows,

- An increase in the air flow rate leads to an increase in the water crossover.
- A higher air flow rate ensures the transportation of the required oxygen concentration in the cell and improves the ORR activity.
- The water crossover increases with increasing current density.
- A lower methanol concentrations and higher current densities ensure low methanol crossover rates.
- A better cell performances are obtained at 0.75 M and 1 M; while lower performances are seen at 0.5 M and 1.25 M.

The remarkable conclusions of short stack performance are listed as follow:

- Better results are obtained at methanol current density of 100 $mA \cdot cm^{-2}$ for all current densities, and average voltage increases about 0.1 V when air flow rate decreases from higher value (30-20 $mL \cdot cm^{-2} \cdot min^{-1}$) to lower (20-10 $mL \cdot cm^{-2} \cdot min^{-1}$) at each current density. It is found that average cell voltage yields 0.36 V for 30 $ml \cdot cm^{-2} \cdot min^{-1}$ air flow rates, 0.37 V for 25 $mL \cdot cm^{-2} \cdot min^{-1}$ air flow rates and 0.38 V for 20 $mL \cdot cm^{-2} \cdot min^{-1}$ air flow rates.

- Average stack voltage reaches a higher value at methanol crossover current density and current density of 50 $mA \cdot cm^{-2}$ and 0.1 $A \cdot cm^{-2}$, respectively.
- Better average cell voltage could be achieved from the stack with decreasing air flow rate just for lower current densities. However, a higher air flow rate provides reliable operation despite the voltage decrement.

The comparison between short stack and cell performance of DMFC was carried out to show the strengths and weaknesses of each of these performances for DMFC characterization. The crucial results derived from this comparison are given as follows:

- Voltage differences between the cells of the short stack increase with increasing current density and methanol concentration. Under these conditions stack temperatures are obtained as very high.
- High methanol permeation leads to a higher voltage loss at cells of the short stack so average cell voltage of the short stack is lower. This could also be due to a loss of heat of the short stack.
- The effort is highest and effects of the heat loss over the stack surfaces is higher for smaller number of cells.

After empirical data are obtained for single cell, they are implemented in the thermodynamic model of the DMFC system. These data are first described as polynomial-form equations using the curve-fitting method. These equations are then coupled to the modelling equations of the DMFC to find the mass flux entering and leaving of the DMFC using Faraday Law, as well as the heat loss and power density of the DMFC. Mass, energy and exergy balances are applied around the control volumes enclosing the BOP components to calculate the electrical and exergetic efficiency of system, power consumption of auxiliary equipment, net power output, condenser outlet temperature, exergy destructions of BOP components and exergetic efficiency of DMFC in cell level.

As a result of this semi-empirical thermodynamic model, the following findings are obtained:

- Decreasing the air flow rate leads to a decrease in the heat duty of the condenser and improves the electrical efficiency of the system.
- The condenser outlet temperature reaches its highest value (47.2 °C) when the current density, air flow rate and concentration are 0.25 $A \cdot cm^{-2}$, 20 $mL \cdot cm^{-2} \cdot min^{-1}$ and 1.25 M, respectively.
- The electrical efficiency gets its highest value as 23.6 % at a current density of 0.20 $A \cdot cm^{-2}$ (It corresponds to 0.387 V), while the methanol concentration is 0.75 M and the air flow rate 20 $mL \cdot cm^{-2} \cdot min^{-1}$.
- The highest power consumption of the system's components occurs in the blower.
- The highest exergy destruction of the system's components occurs in the condenser.
- The exergetic efficiency of system gets the highest value as 27 % at a current density of 0.15 $A \cdot cm^{-2}$ (It corresponds to 0.387 V), while the methanol concentration is 0. 5 M and the air flow rate 30 $mL \cdot cm^{-2} \cdot min^{-1}$.
- The highest exergetic efficiency of DMFC in cell level is found as 60 %.
- With an increase of air flow rate, the exergy destruction of condenser significantly decreases. When the air flow rate increases from 20 $mL \cdot cm^{-2} \cdot min^{-1}$ to 30 $mL \cdot cm^{-2} \cdot min^{-1}$, the exergy destruction rates of condenser increases almost of the 60 % at methanol concentration of 0.5 M while other parameters are taken as constant.
- Both system and cell exergetic efficiency are first increasing at lower current densities for each concentration. After reaching peak point, it decreases with an increasing current density.

In this thermodynamic analysis of DMFC system, the condenser is considered as a black box with some assumptions, generalizations and simplifications. In this case, the system analysis is insufficient to analyse water autonomy. In order to investigate water autonomy in detail, a novel two-phase model of available condenser is first developed at COMSOL Multiphasic 5.4. After comprehensive results are obtained inside the condenser through this model, the mass diffusivity flux which provides water autonomy is calculated, and compared with the system requirements.

The findings of two-phase modelling of condenser is given as follows:

- The saturated gas entering the condenser remains almost saturated during the cooling process. However, it is observed there are noncondensing regions that is below the saturated point.
- The effect of heat transfers due to convection on cooling down of temperature of exhaust gas is very low.
- For this condenser, the mass condensate diffusivity flux of system requirement is higher than condenser ability for variable operating conditions. Therefore, the water autonomy cannot be provided.
- The mass condensate diffusivity flux differences between system requirements and condenser ability decreases when the air flow rate decreases. For example, this differences are found as 0.00003 $kg \cdot s^{-1} \cdot m^2$ and 0.00005 $kg \cdot s^{-1} \cdot m^2$ at air flow rate of 20 $mL \cdot cm^{-2} \cdot min^{-1}$ and 30 $mL \cdot cm^{-2} \cdot min^{-1}$, respectively.

REFERENCES

Albani, M. (2018). *Effects of Operating Conditions on Direct Methanol Fuel Cell*. Master's thesis, Universitat Politècnica de Catalunya, Spain.

Andrian, S. V., & Meusinger, J. (2000). Process analysis of a liquid-feed direct methanol fuel cell system. *Journal of Power Sources, 91*(2), 193–201.

Argyropoulos, P., Scott, K., Shukla, A. K., & Jackson, C. (2003). A semi-empirical model of the direct methanol fuel cell performance: Part I. Model development and verification. *Journal of Power Sources, 123*(2), 190–199.

Ay, M., Midilli, A., & Dincer, I. (2006). Exergetic performance analysis of a PEM fuel cell. *International Journal of Energy Research, 30*(5), 307–321.

Barbir F. (2005). *PEM fuel cells theory and practice*. New York: Elsevier Academic Press.

Bahrami, H., & Faghri, A. (2010). Transport phenomena in a semi-passive direct methanol fuel cell. *International Journal of Heat and Mass Transfer, 53*(11–12), 2563–2578.

Bahrami, H., & Faghri, A. (2011). Exergy analysis of a passive direct methanol fuel cell. *Journal of Power Sources, 196*(3), 1191–1204.

Calabriso, A., Borello, D., Romano, G. P., Cedola, L., Del Zotto, L., & Santori, S. G. (2017). Bubbly flow mapping in the anode channel of a direct methanol fuel cell via PIV investigation. *Applied Energy, 185*, 1245–1255.

Chen, R., & Zhao, T. S. (2005). Mathematical modeling of a passive-feed DMFC with heat transfer effect. *Journal of Power Sources, 152*(1–2), 122–130.

Chiu, Y. J., Yu, T. L., & Chung, Y. C. (2011). A semi-empirical model for efficiency evaluation of a direct methanol fuel cell. *Journal of Power Sources, 196*(11), 5053–5063.

Choi, W. C., Kim, J. D., & Woo, S. I. (2001). Modification of proton conducting membrane for reducing methanol crossover in a direct-methanol fuel cell. *Journal of Power Sources, 96*(2), 411–414.

Colpan, C. O. (2012). Exergy analysis of an integrated two-stage biomass gasifier and Solid Oxide Fuel Cell system. *International Journal of Exergy, 10*(1), 61.

Colpan, C. O., Ouellette, D., Glüsen, A., Müller, M., & Stolten, D. (2017). Reduction of methanol crossover in a flowing electrolyte-direct methanol fuel cell. *International Journal of Hydrogen Energy, 42*(33), 21530–21545.

Corti, H. R., & Gonzalez, E. R. (2014). *Direct alcohol fuel cells: Materials, performance, durability and applications.* In Direct Alcohol Fuel Cells: Materials, Performance, Durability and Applications. Amsterdam: Springer

Cruickshank, J., & Scott, K. (1998). The degree and effect of methanol crossover in the direct methanol fuel cell. *Journal of Power Sources, 70*(1), 40–47.

Dohle, H., Mergel, J., & Stolten, D. (2002). Heat and power management of a direct-methanol-fuel-cell (DMFC) system. *Journal of Power Sources, 111*(2), 268–282.

Dohle, H., & Wippermann, K. (2004). Experimental evaluation and semi-empirical modeling of U/I characteristics and methanol permeation of a direct methanol fuel cell. *Journal of Power Sources, 135*(1–2), 152–164.

Ercelik, M., Ozden, A., Devrim, Y., & Colpan, C. O. (2017). Investigation of Nafion based composite membranes on the performance of DMFCs. *International Journal of Hydrogen Energy, 42*(4), 2658–2668.

Faghri, A., & Guo, Z. (2005). Challenges and opportunities of thermal management issues related to fuel cell technology and modeling. *International Journal of Heat and Mass Transfer, 48*(19–20), 3891–3920.

Faghri, A., & Guo, Z. (2008). An innovative passive DMFC technology. *Applied Thermal Engineering, 28*(13), 1614–1622.

Ge, J., & Liu, H. (2005). Experimental studies of a direct methanol fuel cell. *Journal of Power Sources, 142*(1–2), 56–69.

Guo, Z., & Cao, Y. (2004). A passive fuel delivery system for portable direct methanol fuel cells. *Journal of Power Sources, 132*(1–2), 86–91.

Gwak, G., Kim, D., Lee, S., & Ju, H. (2018). Studies of the methanol crossover and cell performance behaviors of high temperature-direct methanol fuel cells (HT-DMFCs). *International Journal of Hydrogen Energy, 43*(30), 13999–14011.

Hotz, N., Lee, M. T., Grigoropoulos, C. P., Senn, S. M., & Poulikakos, D. (2006). Exergetic analysis of fuel cell micropowerplants fed by methanol. *International Journal of Heat and Mass Transfer, 49*(15–16), 2397–2411.

Hussain, M. M., Baschuk, J. J., Li, X., & Dincer, I. (2005). Thermodynamic analysis of a PEM fuel cell power system. *International Journal of Thermal Sciences, 44*(9), 903–911.

Ince, A. C., Karaoglan, M. U., Glüsen, A., Colpan, C. O., Müller, M., & Stolten, D. (2019). Semiempirical thermodynamic modeling of a direct methanol fuel cell system. *International Journal of Energy Research.*

Ismail, A., Kamarudin, S. K., Daud, W. R. W., Masdar, S., & Hasran, U. A. (2018). Development of 2D multiphase non-isothermal mass transfer model for DMFC system. *Energy, 152*, 263–276.

Izenson, M. G., & Hill, R. W. (2005). Water Balance in PEM and Direct Methanol Fuel Cells. *Journal of Fuel Cell Science and Technology, 2*(1), 1.

Jewett, G., Faghri, A., & Xiao, B. (2009). Optimization of water and air management systems for a passive direct methanol fuel cell. *International Journal of Heat and Mass Transfer, 52*(15–16), 3564–3575.

Jiang, R., & Chu, D. (2006). Power management of a direct methanol fuel cell system. *Journal of Power Sources, 161*(2), 1192–1197.

Jiang, R., & Chu, D. (2008). Water Crossover: A Challenge to DMFC System II. Simulation of Water Recycling in a 20 W DMFC System. *Journal of The Electrochemical Society, 155*(8), B804.

Karaoğlan, M. U., İnce, A. C., Colpan, C. O., Glüsen, A., Kuralay, N. S., Müller, M., & Stolten, D. (2018). Simulation of a hybrid vehicle powertrain having direct methanol fuel cell system through a semi-theoretical approach. *International Journal of Hydrogen Energy*.

Kazim, A. (2004). Exergy analysis of a PEM fuel cell at variable operating conditions. *Energy Conversion and Management, 45*(11–12), 1949–1961.

Knights, S. D., Colbow, K. M., St-Pierre, J., & Wilkinson, D. P. (2004). Aging mechanisms and lifetime of PEFC and DMFC. *Journal of Power Sources, 127*(1–2), 127–134.

Ko, J., Lee, G., Choi, Y., Chippar, P., Kang, K., & Ju, H. (2011). Comparison of numerical simulation results with experimental current density and methanol-crossover data for direct methanol fuel cells. *Journal of Power Sources, 196*(3), 935–945.

Kulikovsky, A. A. (2003). Analytical model of the anode side of DMFC: The effect of non-Tafel kinetics on cell performance. *Electrochemistry Communications, 5*(7), 530–538.

Larminie, J., Dicks, A., & McDonald, M. S. (2003). *Fuel cell systems explained*, 2, 207-225. Chichester, UK: John Wiley.

Lee, J., Lee, S., Han, D., Gwak, G., & Ju, H. (2017). Numerical modeling and simulations of active direct methanol fuel cell (DMFC) systems under various ambient temperatures and operating conditions. *International Journal of Hydrogen Energy*, *42*(3), 1736–1750.

Leo, T. J., Durango, J. A., & Navarro, E. (2010). Exergy analysis of PEM fuel cells for marine applications. *Energy, 35*(2), 1164–1171.

Li, X., & Faghri, A. (2013). Review and advances of direct methanol fuel cells (DMFCs) part I: Design, fabrication, and testing with high concentration methanol solutions. *Journal of Power Sources, 226*, 223–240.

Li, X., He, Y., Yin, B., Miao, Z., & Li, X. (2008). Exergy flow and energy utilization of direct methanol fuel cells based on a mathematic model. *Journal of Power Sources, 178*(1), 344–352.

Liu, F., & Wang, C. Y. (2008). Water and methanol crossover in direct methanol fuel cells-Effect of anode diffusion media. *Electrochimica Acta, 53*(17), 5517–5522.

Lu, G. Q., Liu, F. Q., & Wang, C.-Y. (2004). Water Transport Through Nafion 112 Membrane in DMFCs. *Electrochemical and Solid-State Letters, 8*(1), A1.

Lu, G. Q., Wang, C. Y., Yen, T. J., & Zhang, X. (2004). Development and characterization of a silicon-based micro direct methanol fuel cell. *Electrochimica Acta, 49*(5), 821–828.

Mench, M. M. (2008). *Fuel Cell Engines*. In Fuel Cell Engines. New York: John Wiley & Sons

Mergel, J., Janßen, H., Müller, M., Wilhelm, J., & Stolten, D. (2012). Development of Direct Methanol Fuel Cell Systems for Material Handling Applications. *Journal of Fuel Cell Science and Technology*, *9*(3), 031011.

Moran, M. J., Shapiro, H. N., Boettner, D.D., & Bailey, M. B. (2010). *Fundamentals of engineering thermodynamics*. New York: John Wiley & Sons.

Müller, M., Kimiaie, N., Glüsen, A., & Stolten, D. (2014). The Long Way of Achieving a Durability of 20,000 h in a DMFC System. *Advances in Science and Technology*, *93*, 56–60.

Oliveira, V. B., Rangel, C. M., & Pinto, A. M. F. R. (2009). Modelling and experimental studies on a direct methanol fuel cell working under low methanol crossover and high methanol concentrations. *International Journal of Hydrogen Energy*, *34*(15), 6443–6451.

Osat A., Nejad, E., Sedighi, K., Farhadi, M., & Asghari, F. (2014). Exergy analysis of direct methanol fuel cell based on the experimental setup. *World Applied Sciences Journal, 31*(10), 1847-1856.

Ozden, A., Ercelik, M., Ouellette, D., Colpan, C. O., Ganjehsarabi, H., & Hamdullahpur, F. (2017). Designing, modeling and performance investigation of bio-inspired flow field based DMFCs. *International Journal of Hydrogen Energy*, *42*(33), 21546–21558.

Ramesh, V., & Krishnamurthy, B. (2018). Modeling the transient temperature distribution in a direct methanol fuel cell. *Journal of Electroanalytical Chemistry*, *809*, 1–7.

Ren, X., Springer, T. E., & Gottesfeld, S. (2002). Water and Methanol Uptakes in Nafion Membranes and Membrane Effects on Direct Methanol Cell Performance. *Journal of The Electrochemical Society, 147*(1), 92.

Rice, J., & Faghri, A. (2006). A transient, multi-phase and multi-component model of a new passive DMFC. *International Journal of Heat and Mass Transfer, 49*(25–26), 4804–4820.

Schultze, M., & Horn, J. (2012). *Optimization Approach for Cathode Exhaust Gas Conditioning of a Multifunctional Pem Fuel Cell System for the Application in Aircraft.* Deutscher Luft- Und Raumfahrtkongress, 1–10.

Seo, S. H., & Lee, C. S. (2008). Effect of operating parameters on the direct methanol fuel cell using air or oxygen as an oxidant gas. *Energy and Fuels, 22*(2), 1212–1219.

Sgroi, M. F., Zedde, F., Barbera, O., Stassi, A., Sebastián, D., Lufrano, F & Schuster, M. (2016). Cost analysis of direct methanol fuel cell stacks for mass production. *Energies, 9*(12).

Shaari, N., & Kamarudin, S. K. (2017). Graphene in electrocatalyst and proton conductiong membrane in fuel cell applications: An overview. *Renewable and Sustainable Energy Reviews, 69*, 862–870.

Sun, J., Zhang, G., Guo, T., Jiao, K., & Huang, X. (2018). A three-dimensional multi-phase numerical model of DMFC utilizing Eulerian-Eulerian model. *Applied Thermal Engineering, 132*, 140–153.

Takaguchi, H., & Ohashi, M. (2015). 1 kW Direct Methanol Fuel Cell System. Fujikura Technical Review, 1–4. Retrieved May 9, 2019 from http://www.fujikura.co.jp/eng/rd/gihou/backnumber/pages/__icsFiles/afieldfile/2016/02/16/45e_01_1.pdf

Thomson, G. W. (1946). The antoine equation for vapor-pressure data. *Chemical Reviews*, *38*(1), 1–39.

Vasanth, P., & Kolar, A. K. (2018). Experimental Investigation of Heat Loss from a Passive DMFC using Differential Interferometer. *Fuel Cells*, *18*(2), 195–205.

Wang, L., Yuan, Z., Wen, F., Cheng, Y., Zhang, Y., & Wang, G. (2018). A bipolar passive DMFC stack for portable applications. *Energy*, *144*, 587–593.

Wang, Y., Chen, K. S., Mishler, J., Cho, S. C., & Adroher, X. C. (2011). A review of polymer electrolyte membrane fuel cells: Technology, applications, and needs on fundamental research. *Applied Energy*, *88*(4), 981–1007.

Wu, W., & Lin, Y. T. (2010). Fuzzy-based multi-objective optimization of DMFC system efficiencies. *International Journal of Hydrogen Energy*, *35*(18), 9701–9708.

Xiao, B., & Faghri, A. (2008). Transient modeling and analysis of a passive liquid-feed DMFC. *International Journal of Heat and Mass Transfer*, *51*(11–12), 3127–3143.

Xu, C., & Zhao, T. S. (2007). In situ measurements of water crossover through the membrane for direct methanol fuel cells. *Journal of Power Sources*, *168*(1 SPEC. ISS.), 143–153.

Xu, Q., Zhang, W., Zhao, J., Xing, L., Ma, Q., Xu, L., & Su, H. (2018). Effect of air supply on the performance of an active direct methanol fuel cell (DMFC) fed with neat methanol. *International Journal of Green Energy*, *15*(3), 181–188.

Yang, Q., Kianimanesh, A., Freiheit, T., Park, S. S., & Xue, D. (2011). A semi-empirical model considering the influence of operating parameters on performance for a direct methanol fuel cell. *Journal of Power Sources*, *196*(24), 10640–10651.

Zenith, F., Weinzierl, C., & Krewer, U. (2010). Model-based analysis of the feasibility envelope for autonomous operation of a portable direct methanol fuel-cell system. *Chemical Engineering Science, 65*(15), 4411–4419.

Zhang, J., Yin, G. P., Lai, Q. Z., Wang, Z. B., Cai, K. Di, & Liu, P. (2007). The influence of anode gas diffusion layer on the performance of low-temperature DMFC. *Journal of Power Sources*, *168*(2), 453–458.

APPENDICES

Nomenclature

Abbreviations

ACL	Anode catalyst layer
AGDL	Anode gas diffusion layer
BOP	Balance of Plants
CCL	Cathode catalyst layer
CGDL	Cathode gas diffusion layer
DMFC	Direct Methanol Fuel cell
EES	Engineering Equation Solver
GDL	Gas diffusion layer
M	Membrane
MEA	Membrane electrode assembly
MOR	Methanol Oxidation Reaction
ORR	Oxygen Reduction Reaction
PBI	Polybenzimidazole
PDA	Personal Digital Assistant
PEMFC	Proton Exchange Membrane Fuel Cell
SOFC	Solid Oxide Fuel Cell

Symbols

C	Concentration, M
Ch	Chemical
F	Faraday constant, $A \cdot s \cdot mol^{-1}$
$\overline{ex}_i$	Exergy flow rate of species, $kJ \cdot kmol^{-1}$
h	Enthalpy, $kJ \cdot kg^{-1} \cdot K^{-1}$
i	Current density, $A \cdot cm^{-2}$

LHV	Low Heating Value, $J \cdot m^{-3}$
$\dot{m}''$	mass flux, $kg \cdot h^{-1} \cdot cm^{-2}$
MW	Molecular weight, $kg \cdot kmol^{-1}$
P	Pressure, kPa
$\dot{Q}''$	Heat transfer rate, $W \cdot cm^{-2}$
T	Temperature, °C
Th-Me	Thermo-mechanical
V	Voltage, V
W''	Power density, $W \cdot cm^{-2}$
x	Mole fraction
v	Specific volume flow, $m^3 \cdot kg^{-1}$
λ	Stoichiometric ratio
η	Isentropic efficiency
ρ	Density, $kg \cdot m^{-3}$
φ	Relative humidity ratio
ε	Exergetic efficiency

Subscript/Superscript

a	Anode
aux	Auxiliary
C	Cathode
cond,e	Condenser exit
co	Cathode outlet
cond	Condenser
cons	Consumption
ec	Electro chemical
FC	Fuel cell
gen	Generate
j	Species of fluid
k	Species of auxiliary equipment